Dynamics of Neural Activity During Chemotaxis in Caenorhabditis Elegans

Dynamics of Neural Activity during Chemotaxis in *Caenorhabditis elegans*

A dissertation presented

by

Ching-Han Shen

to

The Department of Molecular and Cellular Biology

in partial fulfillment of the requirements
for the degree of
Doctor of Philosophy
in the subject of
Biology

Harvard University

Cambridge, Massachusetts

May 2015

Dissertation Advisor: Prof. Sharad Ramanathan Ching-Han Shen

Dynamics of Neural Activity during Chemotaxis in *Caenorhabditis elegans*

Abstract

The nervous system of an animal must control and coordinate locomotion in a changing and often unpredictable environment in order to survive. When a *Caenorhabditis elegans* navigates its environment, the nervous system can modulate the animal's behaviors to locate and track chemoattractive gradients to find food. Even though the physical wiring diagram of the nervous system of *C. elegans* was completed 25 years ago, it provides little information as to how interneurons integrate signals to produce complex behavior. Which neurons and what dynamics of activity patterns are important in controlling chemotaxis. Working with Dr. Askin Kocabas and Dr. Zengcai Guo, we used optogenetics and new optical tools to perturb neural activity directly in freely moving animals to evoke chemotactic behavior. We discovered that controlling the activity in just one pair of interneurons (AIY) is sufficient to manipulate the animal to locate, turn towards and track a virtual light gradient. Since AIY interneurons are post-synaptic to most chemosensory neurons, the activity patterns in AIY might be important for signal processing and coordinating locomotion during chemotaxis.

Working with Jeffrey Lee, Dr. Askin Kocabas and Abdullah Yonar, we next investigated how AIY communicates environmental information with its downstream neurons AIZ, RIA, and RIM to control behavior. Using a calcium imaging system built in the laboratory, we found that all of them respond to bacterial odor. Optogenetic stimulation results suggested that AIZ and RIA control gradual turning and RIM controls

reversal. Combining the knowledge from the literature, we proposed a possible functional connection network among neurons important for sensing chemoattractive odor.

Although *C. elegans* only has 302 neurons, we still do not understand how neurons transmit signals nor what role certain neurons have in controlling behavior. The results presented here shed light on the dynamics of the neural activity underlying chemotaxis, and can guide approaches in further research of neural circuits in *C. elegans* and other organisms.

Table of Contents

List of Figures

List of Tables

Acknowledgements

First I would like to thank my advisor, Sharad Ramanathan, for his patience, wisdom and guidance. He has encouraged me to step out of my comfort zone over the last several years to ask questions that matter. As I tumbled through my PhD, he nudged and pushed me through my limits. I thank Sharad for trusting my ability to grow and the willingness to use his time and efforts to mentor me in the best way he can. He taught me that I can learn anything if I am passionate about the question. Confucius said, "A Nobel person's ability is not like a utensil for only one purpose." Sharad showed me exactly that, by pursuing any field that his research interests drove him to. I hope that no matter where I end up in the future, I will still be steered by my curiosity and aspire to solve important problems.

I also want to thank my thesis committee members Jeff Lichtman, Florian Engert and Alex Schier. They have truly listened to me, and have given me very insightful advice for my scientific and personal development. Each of them has a very different approach to science. It is inspiring to know that there can be so many different ways to be successful.

My scientific experience and daily life at Harvard would be so different without the wonderful current and former members in the Ramanathan lab: Askin Kocabas, Jeffery Lee, Sumin Jang, Dann Huh, Leon Furchtgott, Zhechung (Lance) Zhang, Sandeep Choubey, Josselin Milloz, Adele Doyle, Ling-Nan Zou, Yonar Abdullah, Ethan Loew, Jim Valcourt and Steven Zwick. I learnt LabView and setup building from Askin and Jeff. They really know how to communicate engineering and physics ideas in normal English. Sumin, Jeff and Joss have been my constant companions through all the ups and downs.

I cannot think of any PhD program better than The Molecules, Cells and Organisms Program. The Dissertation Annual Committee (DAC) meeting each year helped me refine my research direction. I have been spoiled by well-organized retreats in both the fall and spring terms. Michael Lawrence, Debra Maddalena, Patricia Perez and other administrative staff members know the answers to all my questions, as well as to the questions I should have asked.

I want to thank Xiuye Chen and Laila Akhmetova for going through all the ups and downs with me. I will remember the nights we discussed about science and life and everything in between. I also thank all my volleyball friends who keep me in shape. Particular thanks to Sasha Johnson-Freyd for going with me through so far the most challenging period of my life.

My family has been a constant source of unconditional love and support. My mom is always wise and right, including that writing a thesis would be more difficult than I had thought. My dad has had constant support and 100% confidence in me. My grandmother is a genius and an inventor in her own way. I always think of her as my role model and inspiration to keep going and to keep asking questions. My sister is my best companion for running through any crazy ideas. My cousin Tina brought me to the field of neurobiology and has given me much good advice.

Many people have helped me to get to where I am. There are more people and events I would like to thank. Please forgive me for not listing here. I am grateful to all the encounters and warm memories I have had with you.

To

my mother Pei-Chun Shen (沈珮君)

my father Ying-Ming Lin (林營明)

and

my grandmother Feng-Chin Chen (陳鳳金)

Chapter 1. Overview

1.1. *C. elegans* as a model organism

C. elegans is a major model organism in biological research[1,2]. The animal can be cultured in the laboratory where it grows on agar plates with *Escherichia coli* as a food source. In nature, it is a freely-living nematode that can be found in soil and decaying organic matters. The animal is 1 mm long as an adult. The life cycle of *C. elegans* is around 3 days under optimal conditions. Most of the *C. elegans* are hermaphrodites and only a small portion of them are males. As a result, self-fertilization of hermaphrodites generates genetically identical progenies and male mating can produce progenies with different genetic backgrounds. *C. elegans* has many advantages for neuroscience studies. The animal is transparent and therefore is easy to observe and manipulate with optics. It has a small neural network with 302 invariant neurons and the physical connections between neurons have been mapped[3,4]. Despite its relative simplicity of study, *C. elegans* displays complex behaviors such as chemotaxis, male mating, learning and social behaviors[5,6]. Therefore, it is a powerful model organism to study the dynamics of neural activity underlying behaviors.

1.2. Behavior of *C. elegans*

Complex behaviors in *C. elegans* are generated from a relatively simple locomotive repertoire. The animal crawls on its side, generating sinusoidal movement by alternating contraction of its dorsal and ventral sides to go forward and backward. To change the direction of forward movement, *C. elegans* produces larger head swing on one side to curve its trajectory toward that direction (gradual turning)[7]. Alternatively, the animal can also reorient itself by pausing, swinging its head to touch its tail to form the

shape omega (omega turn), or coupling reversal and omega turn to perform a pirouette[8–10]. Literature uses various terms to describe the behaviors above. For convenience of discussion, we use "reversals" to describe behaviors that lead to abrupt change of reorientation, such as omega turns and pirouettes.

C. elegans modulates its locomotion during chemotaxis. When the animal is moved from a bacterial lawn to a location far away from its food source, it reverses frequently and moves locally near where it is placed. After 10~15 minutes, the animal begins to move away from its original place with decrease of reversal frequency and increase of forward movement align with the direction of the food[8]. As the animal gets closer to food, it adjusts its head swing angle to gradually turn towards the bacterial lawn (Figure 1.1)[7,9]. Therefore, to successfully chemotax to a food source, the animal modulates its locomotion based on the time spent in a given environment and signals received from the environment.

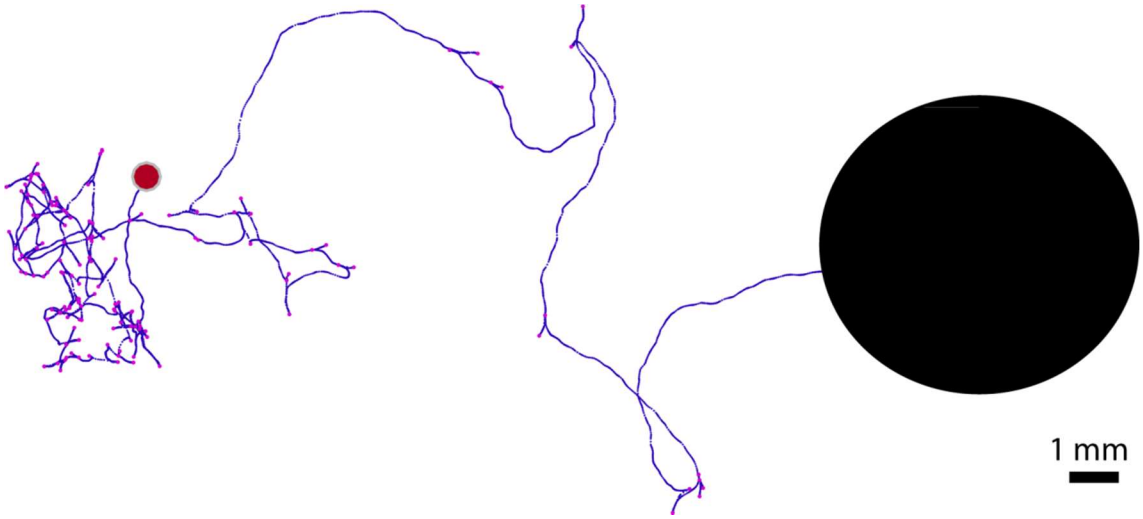

Figure 1.1: A sample trajectory of *C. elegans* chemotax to a bacterial lawn. Blue line represents the trajectory of the center of mass of an animal; red dot represents the animal's starting position; magenta dots represent reversal events; black circle is the bacterial lawn.

C. elegans senses both soluble chemicals and volatile odors secreted from a bacterial lawn for chemotaxis[11]. The animal has been found to respond to a few water-soluble attractants, such as Na^+, Cl^-, cAMP and biotin, as well as a broad spectrum of volatile odors such as alcohols, ketones, esters and aromatic compounds[12,13]. The animal's response to volatile odors is more sensitive (10^{-9} M) than that to water-soluble attractants (10^{-3}~10^{-6} M). Based on these findings, some have argued that *C. elegans* uses odor cues for long-range chemotaxis and water-soluble cues for short-range chemotaxis[14]. Interestingly, there are only two classes of chemosensory neurons that respond to odors, whereas there are many classes of chemosensory neurons that respond to water-soluble attractants[14]. What is the significance of the discrepancy? Does the nervous system use different computation methods for water-soluble chemicals and volatile odors? What happens if the animal receives signals from both modalities? These sensory neurons connect to the same sets of interneurons. How do the interneurons compute the information from different sensory inputs? These observations suggest that the dynamics of neural activity underlying chemotaxis might be very complex. Below I will describe what we know about the nervous system from the literature.

1.3. Nervous system of *C. elegans*

The positions of neurons and physical connections between them in *C. elegans* have been reconstructed by serial electron micrography[3]. Hermaphrodites have 302 neurons, with highly consistent morphology and structure among individuals[4]. Each neuron has been given a unique name and can be distinguished from others. Neurons with similar morphologies and synaptic connections are grouped together into 118 classes. In many cases, a single class represents a pair of bilaterally symmetric neurons. The neurons

can also be categorized functionally into sensory, inter- and motor neurons. Sensory neurons perceive environmental cues; interneurons process inputs and relay outputs to other neurons; and motor neurons are synaptically connected to muscles.

The structure of the nervous system provides insights into the function of individual neurons. For example, interneurons AIA, AIY and AIZ receive most of their inputs from sensory neurons and have been identified as important neurons in sensing chemicals[7,14–17]. Interneurons AVA, AVD, AVE and PVC synapse to many motor neurons and are involved in controlling the animal's forward and backward movement[18].

However, the wiring diagram does not include all the information we need to predict how the nervous system processes signals. Every neuron has on average more than 20 connections of varied strength, so we cannot predict how the information from one neuron is relayed to the downstream neurons (Figure 1.2)[19]. To understand how the neurons process information, we also need to know whether the connections are excitatory or inhibitory, how strong the connections are and the electrophysiology of the neurons.

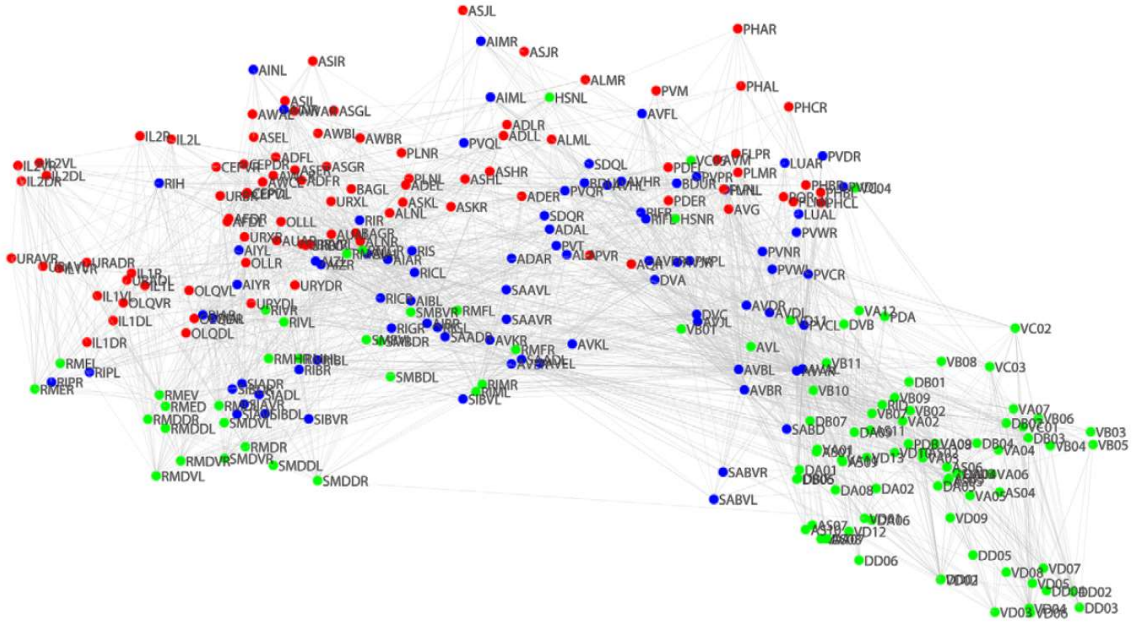

Figure 1.2: Diagram of the physical wiring of the neurons in *C. elegans*. Red dots represent sensory neurons, blue dots represent interneurons, and green dots represent motor neurons. Grey lines represent the physical connections between neurons. However, the strengths of the connections are not known. Adapted from Varshney *et al.,* 2011.

Not only are the functional connections between neurons more complex than the wiring diagram suggests, but we also know very little about the detailed electrophysiology of individual neurons in *C. elegans*[20]. First, due to the lack of voltage-gated sodium channels in *C. elegans*, the nervous system might transmit signals in a different way from the neurons in vertebrates[21]. Second, electrophysiology recordings show diverse activity patterns across different classes of neurons in *C. elegans.* For example, sensory neuron pair ASE is isopotential but has high sensitivity to small currents (2~4 pA)[22], whereas motor neuron class RMD shows spontaneous fluctuation between two potentials[23]. Third, genome of *C. elegans* encodes more than 70 different potassium channels, which suggests the activity patterns of neurons can be regulated in a very diverse way. These findings suggest that the activity patterns can be very different in each neuron. However, in most neurons, we do not know what their activity patterns are.

Even in the neurons that were recorded, we do now know what behaviors the activity patterns correlate with.

1.4. Neurons involved in chemotaxis

C. elegans senses water-soluble chemicals and volatile odors by the cilia of chemosensory neurons[3]. Neurons required for different chemical cues have been identified through laser ablation and some of their responses have been recorded by calcium imaging. Table 1.1 summarizes the key chemosensory neurons involved in chemotaxis.

Table 1.1: Chemosensory neurons involved in chemotaxis and experiment evidence

Neuron	Method	Result
AWA	Laser ablation	Defective chemotaxis to diacetyl and pyrazine[13]
	Calcium imaging	Increase: addition of diacetyl, pyrazine, 2,4,5-trimethylthiazole, 2-methylpyrazine, and hexyl acetate[17]
AWC	Laser ablation	Defective chemotaxis to benzaldehyde, 2-butanone, isoamyl alcohol[13] Decrease reversal frequency[8]
	Calcium imaging	Increase: Removal of isoamyl alcohol, benzaldehyde and bacteria supernatant Decrease: Addition of isoamyl alcohol and bacteria supernatant[15,24]
ASE	Laser ablation	Defective chemotaxis to Na^+, Cl^-, cAMP, biotin, lysin and serotonin[25] Unable to use gradual turning and reversals to find gradient[7]
ASEL	Calcium imaging	Increase: Increase of NaCl; addition of bacteria supernatant[24,26] Decrease: Removal of bacteria supernatant[24]
ASER	Calcium imaging	Increase: Removal of bacteria supernatant[24] Decrease: Increase of NaCl[26]

The wiring diagram shows that sensory neurons ASE, AWA and AWC have many chemical synapses connecting to interneurons AIA, AIB, AIY, AIZ and RIA based

on the wiring diagram. Previous studies from laser ablation, genetic manipulation and calcium imaging have provided clues of their functions in chemotaxis as summarized in Table 1.2.

Table 1.2: Interneurons involved in chemotaxis and experiment evidence

Neuron	Method	Result
AIA	Laser ablation	Increase reversal frequency[8,16]
	Calcium imaging	Increase: addition of diacetyl Decrease: removal of diacetyl[17]
AIB	Laser ablation	Decrease reversal frequency[8]
	Calcium imaging	Increase: Removal of isoamyl alcohol Decrease: addition of isoamyl alcohol[15]
AIY	Laser ablation	Increase reversal frequency[8,16,27]
	Calcium imaging	Increase: addition of diacetyl, isoamyl alcohol Decrease: removal of diacetyl isoamyl alcohol[15,17]
AIZ	Laser ablation	Unable to use gradual turning and reversals to chemotax[7] Decrease reversal frequency[8,27]
RIA	Laser ablation	Decrease reversal frequency[8]
	Calcium imaging	Increase: removal of isoamyl alcohol Decrease: addition of isoamyl alcohol[28]

Interneurons AIA, AIB, AIY, AIZ and RIA process information from sensory neurons and relay it to neurons controlling locomotion. However, the circuit is complicated: Neurons connect with each other in many different paths and we cannot predict how the information flows from sensory neurons to inter- and motor neurons by simply looking at the wiring diagram (Figure 1.3).

Figure 1.3: Wiring diagram of inter- and motorneurons involved in chemotaxis. Triangles represent sensory neurons; hexagons represent interneurons; and circles represent motor neurons. Red and orange lines represent monadic and polyadic synapses, respectively and blue lines are gap junctions. The thickness of the lines is proportional to synapse number.

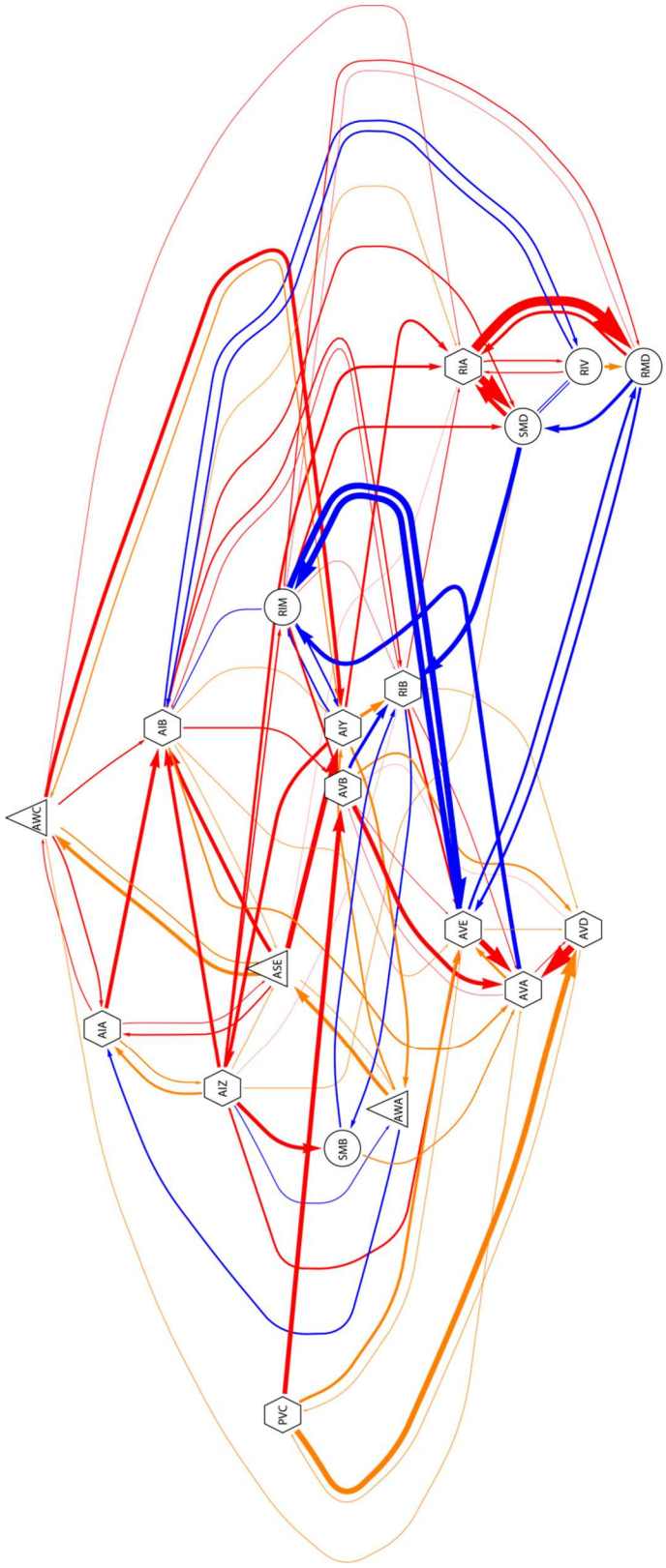

Figure 1.3 (Continued)

In addition, the dynamics of the circuit might be different based on the locomotion and the state of the animal. To understand the functions of these neurons, it is important to perturb or to observe the activity of neurons while the animal is freely moving. This is a necessary approach to provide behavior context. We cannot know if the activity patterns are physiologically relevant without knowing what behaviors that are correlated with.

1.5. Tools to perturb and monitor neural activity in *C. elegans*

Neural activity can be perturbed temporarily when light-gated ion channels are expressed in the neurons in *C. elegans*[29–31]. The ion channels are activated within milliseconds upon illumination with specific wavelengths of light[32,33]. For example, Channelrhodopsin-2 (ChR2) is a non-specific cation channel that depolarizes neurons with maximum activation at 480 nm, while Archaerhodopsin-3 (Arch) is an anti-proton pump that hyperpolarizes neural activity when driven by blue-green light. There are also variants of light-gated ion channels with different ion selectivity, kinetics, photocurrent amplitude and wavelengths[34].

We use calcium transients as a proxy of neural activity in order to understand the functional connections of the neural circuit. Genetically encoded calcium indicators have been developed to report calcium concentration change. It has the advantage of expressing in specific cell types and non-invasive compared to calcium dyes. Both single wave length sensor GCaMP and Forster resonance energy transfer indicators (FRET) are widely used[35,36]. We use GCaMP for calcium imaging so that we can use other wavelength for other purposes.

GCaMP is designed based on circular permuted green fluorescence protein (cpGFP), a calcium-binding protein (calmodulin) and a peptide chain (M13). In the absence of free calcium, the conformation of cpGFP emits little fluorescence under 488 nm; whereas in the presence of free calcium, CaM binds to calcium and changes the conformation of cpGFP by binding to M13 and emits strong fluorescence. GCaMP has been engineered for many generations since its invention to increase its speed and sensitivity. For example, GCaMP6s has low baseline fluorescence and calcium binding form is 27% brighter than enhanced GFP[37]. It can detect single action potentials in many brain region and the rise and decay time of GCaMP also has significant improvement over generations.

Genetically encoded voltage sensors have also been developed[38]. They have the advantage of directly reporting voltage and fast kinetics. However, the current version of genetically encoded voltage sensors suffers from weak fluorescence and limited dynamic range. It might not be applicable to record the neural activity changes in *C. elegans.*

1.6. Future directions

Combining optogenetic tools and the optical system developed in the laboratory, we perturbed the activity of neurons while the animal is freely moving in Chapter 2. We showed that it is important to consider the movement of the animal and the perturbation can have different results based on the motion of the animal. The ability to perturb activity in any desired temporal and spatial patterns opens up many questions. Does the same neuron control different behaviors based on the environmental cues? What are the differences in perturbing the animal when the animal is on the bacterial lawn versus away from it? What happens if we perturb the activity of important neurons while the animal

searches for food? In addition, many neurons in the nervous system of *C. elegans* have not been investigated in details due to the lack of specific promoters. With spatial stimulation, we can now study the function of those neurons and understand the neural circuits with a more complete picture.

However, we cannot control the strength of optogenetic stimulation precisely since the expression level of the light-gated ion channel varies from animal to animal. Therefore, it is important to image the activity of neurons when the animal moves freely. Our lab developed an optical system to measure the calcium activity of neurons of interest in a freely moving animal. We used the system to measure the activity of AIY and neurons upstream and downstream during chemotaxis or with odor delivery in Chapter 3. Though controlling the activity of AIY can evoke chemotactic behavior, we could not even predict if the animal successfully chemotaxed to the food based on the activity changes of AIY. How is the information from the environment encoded in neural activity? Should we look at the absolute level of the activity or the slope of the changes of activity? Should we observe the activity in multiple neurons for more clues? What are the behavioral correlates of the activity patterns in neurons? Is calcium activity even the proper indicator to measure?

We now have tools to perturb and monitor activity of neurons in freely moving animal to address these questions. Chapter 3 presents some observations we made and the research we would like to take on. Understanding the functional connectivity of the interneurons can provide some insights in the underlying dynamics of neural activity during chemotaxis in *C. elegans.*

Reference

1. Brenner, S. & Ls, D. P. F. J. The genetics of behaviour. *Prospects* **29,** 269–271

2. Brenner, S. Caenorhabdztzs elegans. *Methods* 71–94 (1974).

3. White, J., Southgate, E., Thomson, J. N. & Brenner, S. The structure of the nervous system of the nematode Caenorhabditis elegans. *Phil. Trans. Royahl Soc. Lond. B* **314,** 1–340 (1986).

4. Sulston, J. E., Schierenberg, E., White, J. G. & Thomson, J. N. The embryonic cell lineage of the nematode Caenorhabditis elegans. *Developmental biology* **100,** 64–119 (1983).

5. De Bono, M. & Maricq, A. V. Neuronal substrates of complex behaviors in C. elegans. *Annual review of neuroscience* **28,** 451–501 (2005).

6. Ardiel, E. L. & Rankin, C. H. An elegant mind: learning and memory in Caenorhabditis elegans. *Learning & memory (Cold Spring Harbor, N.Y.)* **17,** 191–201 (2010).

7. Iino, Y. & Yoshida, K. Parallel use of two behavioral mechanisms for chemotaxis in Caenorhabditis elegans. *The Journal of neuroscience : the official journal of the Society for Neuroscience* **29,** 5370–80 (2009).

8. Gray, J. M., Hill, J. J. & Bargmann, C. I. A circuit for navigation in Caenorhabditis elegans. *Proceedings of the National Academy of Sciences of the United States of America* **102,** 3184–91 (2005).

9. Pierce-Shimomura, J. T., Morse, T. M. & Lockery, S. R. The fundamental role of pirouettes in Caenorhabditis elegans chemotaxis. *The Journal of neuroscience : the official journal of the Society for Neuroscience* **19,** 9557–69 (1999).

10. Salvador, L. C. M., Bartumeus, F., Levin, S. A., Ryu, W. S. & Valle, C. Caenorhabditis elegans Mechanistic analysis of the search behaviour of Caenorhabditis elegans. (2014).

11. Ps, G. & Dj, W. Migration of Caenorhabditis elegans larvae towards bacteria and the nature of the bacterial stimulus. *Fundamental and Applied Nematology* **15,** 159–166 (1992).

12. Bargmann, C. I. & Horvitz, H. R. Chemosensory Neurons with Overlapping Direct Chemotaxis to Multiple Chemicals in C . elegans. *Cell* **7,** 729–742 (1991).

13. Bargmann, C. I., Hartwieg, E. & Horvitz, H. R. Odorant-selective genes and neurons mediate olfaction in C. elegans. *Cell* **74,** 515–27 (1993).

14. Bargmann, C. I. Chemosensation in C. elegans. *WormBook : the online review of C. elegans biology* 1–29 (2006). doi:10.1895/wormbook.1.123.1

15. Chalasani, S. H. *et al.* Dissecting a circuit for olfactory behaviour in Caenorhabditis elegans. *Nature* **450,** 63–70 (2007).

16. Wakabayashi, T., Kitagawa, I. & Shingai, R. Neurons regulating the duration of forward locomotion in Caenorhabditis elegans. *Neuroscience research* **50,** 103–11 (2004).

17. Larsch, J., Ventimiglia, D., Bargmann, C. I. & Albrecht, D. R. High-throughput imaging of neuronal activity in Caenorhabditis elegans. *Proceedings of the National Academy of Sciences of the United States of America* **110,** E4266–73 (2013).

18. Chalfie, M. *et al.* The neural circuit for touch sensitivity in Caenorhabditis elegans. *The Journal of neuroscience : the official journal of the Society for Neuroscience* **5,** 956–64 (1985).

19. Varshney, L. R., Chen, B. L., Paniagua, E., Hall, D. H. & Chklovskii, D. B. Structural Properties of the Caenorhabditis elegans Neuronal Network. *PLoS Computational Biology* **7,** e1001066 (2011).

20. Goodman, M. B., Lindsay, T. H., Lockery, S. R. & Richmond, J. E. *Electrophysiological methods for Caenorhabditis elegans neurobiology. Methods in cell biology* **107,** 409–36 (Elsevier Inc., 2012).

21. Bargmann, C. I. Neurobiology of the Caenorhabditis elegans genome. *Science (New York, N.Y.)* **282,** 2028–2033 (1998).

22. Goodman, M. B., Hall, D. H., Avery, L. & Lockery, S. R. and Dynamic Range in C . elegans Neurons. **20,** 763–772 (1998).

23. Mellem, J. E., Brockie, P. J., Madsen, D. M. & Maricq, A. V. Action potentials contribute to neuronal signaling in C. elegans. *Nature neuroscience* **11,** 865–7 (2008).

24. Zaslaver, A. *et al.* Hierarchical sparse coding in the sensory system of Caenorhabditis elegans. *Proceedings of the National Academy of Sciences* **112,** 1185–1189 (2015).

25. Bargmann, C. I. & Horvitz, H. R. Control of larval development by chemosensory neurons in Caenorhabditis elegans. *Science (New York, N.Y.)* **251,** 1243–6 (1991).

26. Miller, A. C., Thiele, T. R., Faumont, S., Moravec, M. L. & Lockery, S. R. Step-response analysis of chemotaxis in Caenorhabditis elegans. *The Journal of neuroscience : the official journal of the Society for Neuroscience* **25,** 3369–78 (2005).

27. Tsalik, E. L. & Hobert, O. Functional mapping of neurons that control locomotory behavior in Caenorhabditis elegans. *Journal of neurobiology* **56,** 178–97 (2003).

28. Hendricks, M., Ha, H., Maffey, N. & Zhang, Y. Compartmentalized calcium dynamics in a C. elegans interneuron encode head movement. *Nature* **487,** 99–103 (2012).

29. Nagel, G. *et al.* Light activation of channelrhodopsin-2 in excitable cells of Caenorhabditis elegans triggers rapid behavioral responses. *Current biology : CB* **15,** 2279–84 (2005).

30. Okazaki, A., Sudo, Y. & Takagi, S. Optical silencing of C. elegans cells with arch proton pump. *PloS one* **7,** e35370 (2012).

31. Zhang, F. *et al.* Multimodal fast optical interrogation of neural circuitry. *Nature* **446,** 633–9 (2007).

32. Boyden, E. S., Zhang, F., Bamberg, E., Nagel, G. & Deisseroth, K. Millisecond-timescale, genetically targeted optical control of neural activity. *Nature neuroscience* **8,** 1263–8 (2005).

33. Chow, B. Y. *et al.* High-performance genetically targetable optical neural silencing by light-driven proton pumps. *Nature* **463,** 98–102 (2010).

34. Berndt, A. *et al.* High-efficiency channelrhodopsins for fast neuronal stimulation at low light levels. *Proceedings of the National Academy of Sciences of the United States of America* **108,** 7595–600 (2011).

35. Tian, L. *et al.* Imaging neural activity in worms, flies and mice with improved GCaMP calcium indicators. *Nature methods* **6,** 875–81 (2009).

36. Thestrup, T. *et al.* Optimized ratiometric calcium sensors for functional in vivo imaging of neurons and T lymphocytes. *Nature methods* (2014). doi:10.1038/nmeth.2773

37. Chen, T.-W. *et al.* Ultrasensitive fluorescent proteins for imaging neuronal activity. *Nature* **499,** 295–300 (2013).

38. Kralj, J. M., Hochbaum, D. R., Douglass, A. D. & Cohen, A. E. Electrical spiking in Escherichia coli probed with a fluorescent voltage-indicating protein. *Science (New York, N.Y.)* **333,** 345–8 (2011).

Chapter 2. Controlling interneuron activity in Caenorhabditis elegans to evoke chemotactic behavior

[A large part of this chapter is published as "Controlling interneuron activity in Caenorhabditis elegans to evoke chemotactic behaviour", Askin Kocabas, Ching-Han Shen, Zengcai V. Guo, Sharad Ramanathan, Nature, 490, 273-278 (2012). A.K. designed and built the optical setups, planned and performed experiments and wrote manuscript. C.-H.S. made transgenic lines, planned and performed experiments and wrote manuscript. Z.V.G. made transgenic lines, performed experiments. S.R. planned experiments and wrote manuscript.]

Abstract

Animals locate and track chemoattractive gradients in the environment to find food. With its small nervous system, *Caenorhabditis elegans,* is a good model system in which to understand how the dynamics of neural activity control this search behavior. Extensive work on the nematode has identified the neurons that are necessary for the different locomotory behaviors underlying chemotaxis through laser ablation, activity recording in immobilized animals and the study of mutants. However, we do not know the neural activity patterns in *C. elegans* that are sufficient to control its complex chemotactic behavior. To understand how the activity in its interneurons coordinates different motor programs to lead the animal to food, we used optogenetics and new optical tools to directly manipulate neural activity in freely moving animals to evoke chemotactic behavior. By deducing the classes of activity patterns triggered during chemotaxis and exciting individual neurons with these patterns, we identified

interneurons that control the essential locomotory programs for this behavior. Surprisingly, we discovered that controlling the dynamics of activity in just one interneuron pair (AIY) was sufficient to force the animal to locate, turn towards and track virtual light gradients. Two distinct activity patterns triggered in AIY as the animal moved through the gradient, controlled reversals and gradual turns to drive chemotactic behavior. Since AIY are post-synaptic to most chemosensory and thermosensory neurons, these activity patterns in AIY are likely to play an important role in controlling and coordinating different taxis behaviors of the animal.

2.1. Introduction

Organisms, from bacteria to multicellular eukaryotes, have to search for food to survive. Complex internal circuits process external signals to evoke and coordinate multiple motor programs, leading the animal to track attractive odors and find food. Are there master nodes in the circuits that control and coordinate search behavior? Here we ask if the neural circuits generating chemotactic behavior in *C. elegans* can be controlled through such key nodes.

The nematode *C. elegans* uses reversals (backward movement), sharp and gradual turns to locate, and track gradients of chemo-attractive signals[1–4]. Previous work on *C. elegans* has identified about 14 pairs of inter and motor neurons including the interneurons AIY, AIZ and AIB that are necessary for the locomotory behaviors underlying chemotaxis (Table 2.1)[1–3,5–8]. The neuro-anatomy of the animal shows that a majority of the amphid chemosensory and thermosensory neurons synapse onto one or more of the first layer of interneuron pairs AIY, AIZ, and AIB[9], which are further connected to a dense network of interneurons[8]. The activity dynamics in this network

must process sensory signals to produce and coordinate the different locomotory behaviors underlying chemotaxis through the downstream motor neurons. Despite the experiments in the literature involving ablation, genetics, and calcium imaging, we do not know if chemotaxis is driven by key interneurons or if the generation of this complex behavior is achieved by the dynamics of a more diffuse neural network.

Table 2.1: Literature summary of behavioral defects upon inter- and motor-neuron ablations

Ablated neurons	Behavioral defects
AIB	reversals and omega turns decreased[7]
AIY	persistent reversals and omega turns, unclear about gradual turning[1,5,7]
AIZ	reversals decreased[10], gradual turning abolished[1]
RIB	reversal frequency and omega turns increased[5,7]
RIV	omega turns decreased, eliminates ventral bias of omega turns[7]
RIM	reversals decreased[5,7]
AVA	reversals decreased[7]
AVB	reversals increased[11]
AVA + AVD	inability to move backward[11]
AVB + PVC	inability to move forward[11]
SMB	head-bending angle increased, loopy and high-amplitude sinusoidal movement[7]
SMD	omega turns reduced, reversal frequency increased, amplitude of omega turn decreased[7]
RMD	reversal frequency increased[7]
RME	head bending angle increased, loopy movement

2.2. Results

2.2.1. Deduce the activity patterns triggered during chemotaxis

To evoke chemotactic behavior by directly controlling interneuron activity, we have to answer two intricately linked questions: which sets of interneurons do we control, and what activity patterns do we stimulate in them? To deduce the classes of activity patterns triggered in the nervous system during chemotaxis, we followed animals as they crawled towards a bacterial lawn (Figure 2.1a). The undulatory head swings (from dorsal to ventral, since the animal crawls on its side) caused the angle at which the head bends relative to the locomotory direction, $h(t)$ (Figure 2.1b), to oscillate between positive and negative values. Due to this changing head-bending angle and the movement of the animal, sensory cilia at the nose tip experienced the spatial profile of the chemoattractants (Figure 2.1a-b) as a temporally fluctuating odor signal, $I(h,t)$. In general, this signal can be written as a sum of two terms $I(h,t) = S_I(h,t) + A_I(h,t)$, where S_I is a symmetric function of h : $S(h,t) = S(-h,t)$ and A_I is an asymmetric function of h : $A(h,t) = -A(-h,t)$. When the animal moves perpendicular to the gradient direction I is dominated by A_I (Figure 2.1b-d, top). As the animal turns and tracks the gradient, the magnitude of A_I , $|A_I|$decreases and I is dominated by S_I (Figure 2.1b-d, bottom).

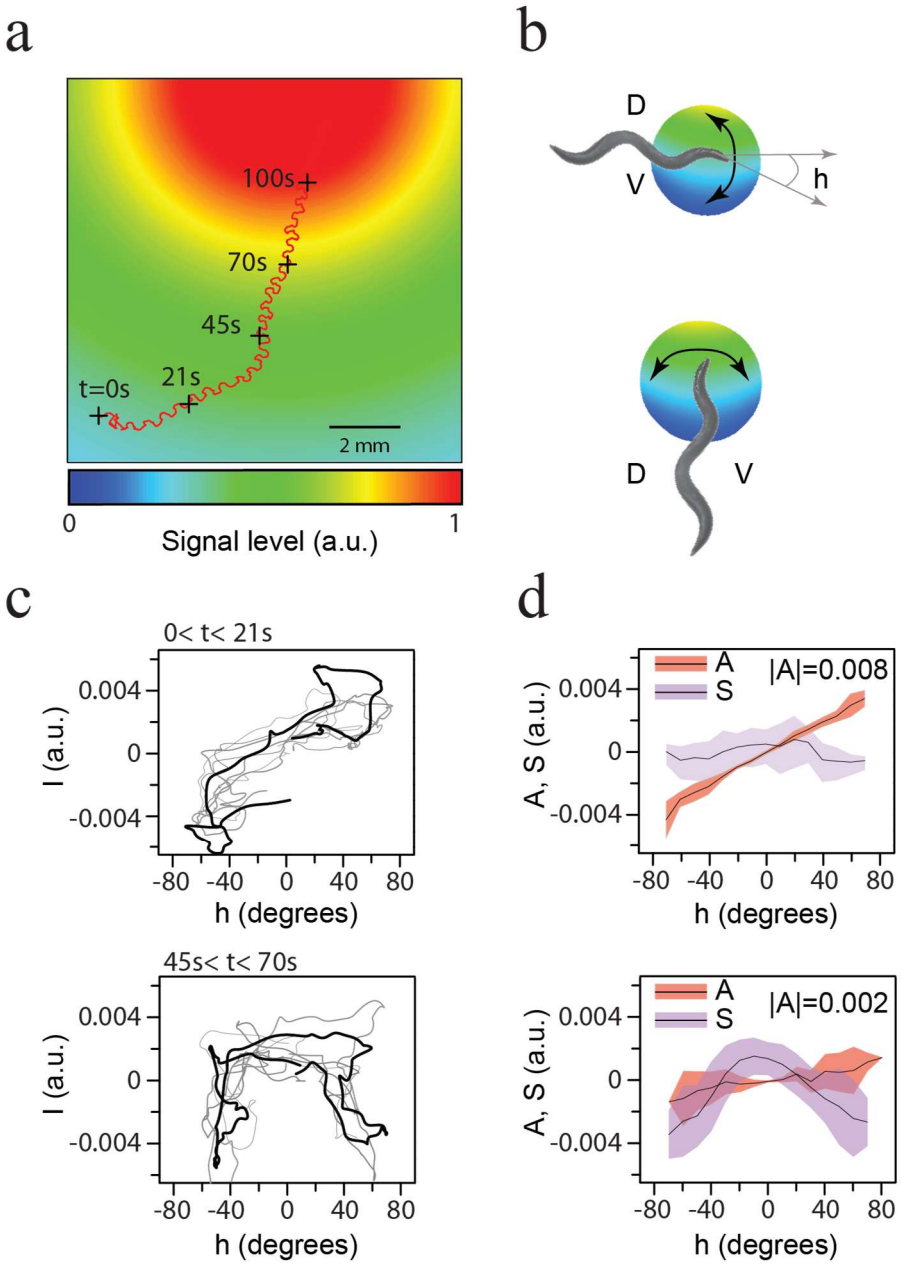

Figure 2.1: Asymmetric component of the odor signal controls gradual turning. a, Trajectory of a nematode's nose tip overlaid on modeled exponential profile (decay length 1 cm) of the gradient of chemoattractants (pseudocolor) from the bacterial lawn. Plus signs: positions of animal at indicated times. a.u.: arbitrary units. **b,** Illustration of an animal crawling perpendicular to (above) and along (below) the odor gradient. h: head-bending angle; D: dorsal ($h>0$); V: ventral ($h<0$). **c,** Odor signal at nose tip, $I(t)$, vs. head-bending angle, $h(t)$, over the last (black) and sequentially prior (grey) head swings for the nose-tip trajectory in (**a**). **d,** Plot of the mean and s.d. of the asymmetric ($A(t)$) and symmetric ($S(t)$) components of $I(t)$ in (**c**). |A|: magnitude of $A(t)$.

2.2.2. Asymmetric component of the odor signal controls gradual turning

To determine how these asymmetric and symmetric components of $I(t)$ controlled locomotory behavior, we built a microscopy system that delivered odors on a freely crawling animal in precise temporal patterns determined by $h(t)$ (Figure 2.2a). To mimic A_1 , we exposed the animal to asymmetric odor stimulation: air with chemoattractant vapors (10^{-3} M isoamyl alcohol) blown on the entire animal when the head was bent in one direction (for example, dorsally, $h > 0$) and odor-free air blown when the head was bent in the other (ventrally, $h < 0$) (Figure 2.2b). The animal turned gradually in the direction in which its head was bent when the odor was delivered (Figure 2.2c). To mimic S_1 we delivered vapors of isoamyl alcohol constantly independent of h. The animal reduced its reversal frequency[9] and did not turn (Figure 2.2d). The most parsimonious hypothesis based on these results is that asymmetric and symmetric odor components generate activity patterns in the nervous system with corresponding symmetries to separately control turning and reversal frequency during chemotaxis.

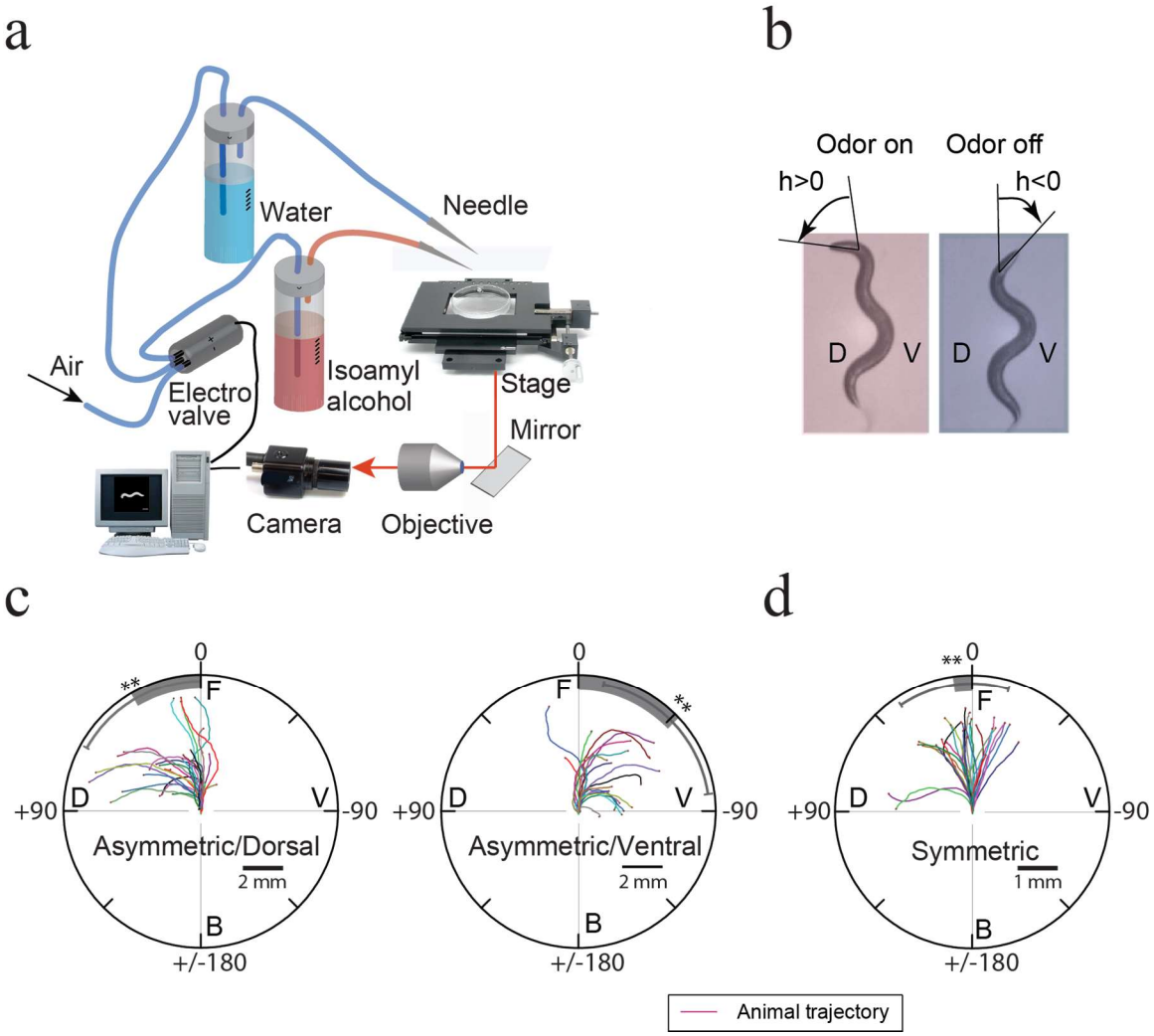

Figure 2.2: Asymmetric odor stimulation causes gradual turning. a, A closed-loop control system for odor delivery. Based on the animal's posture, obtained by automated image processing at 20Hz by a customized worm tracker, the computer controlled an electric valve to determine whether air was bubbled through 10^{-3} M isoamyl alcohol (red tube) or through water (blue tube) before being gently blown on the freely moving animal. **b**, Dorsal asymmetric odor stimulation. **c-d,** Sample trajectories of center of mass of the animals upon (c) dorsal and ventral asymmetric, (d) symmetric odor stimulation. Grey bar: mean turning angle; D: dorsal; V: ventral; F: front; B: back; angles (0, 90, -90, 180) define the turning angles with respect to initial orientation of animal. n=10; **, $p<0.05$, two-sample t-test.

2.2.3. Asymmetric and symmetric excitation of AIY control gradual turning and reversal frequency

We therefore identified interneurons that triggered the different locomotory behaviors necessary for chemotaxis by directly stimulating individual neurons in a freely moving animal in asymmetric and symmetric patterns. To do so, we expressed channelrhodopsin-2 (ChR2)[12,13] or archaerhodopsin-3 (Arch)[14,15] in different neurons. Light activation of ChR2 (by 480 nm light) and Arch (540 nm) leads to neural excitation and inhibition, respectively.

Targeted illumination of specific neurons in motionless animals[16] or of body segments in freely moving animals[10,17] have been developed to excite neurons for which specific promoters are not known. Since the neurons in the nerve ring are as close as 5-10 mm to each other and their relative positions change quickly as the animal moves (Figure 2.3a), we could not use these techniques. To optically stimulate one of many neurons (each with a diameter of 5-10 μm) expressing light-gated ion channels in the nerve ring of an animal that typically moves at 150±50 μm/s, our setup tracks, identifies, and specifically illuminates the neuron(s) of interest, all within 25 milliseconds to achieve a 5 μm spatial resolution of excitation (Figure 2.3b).

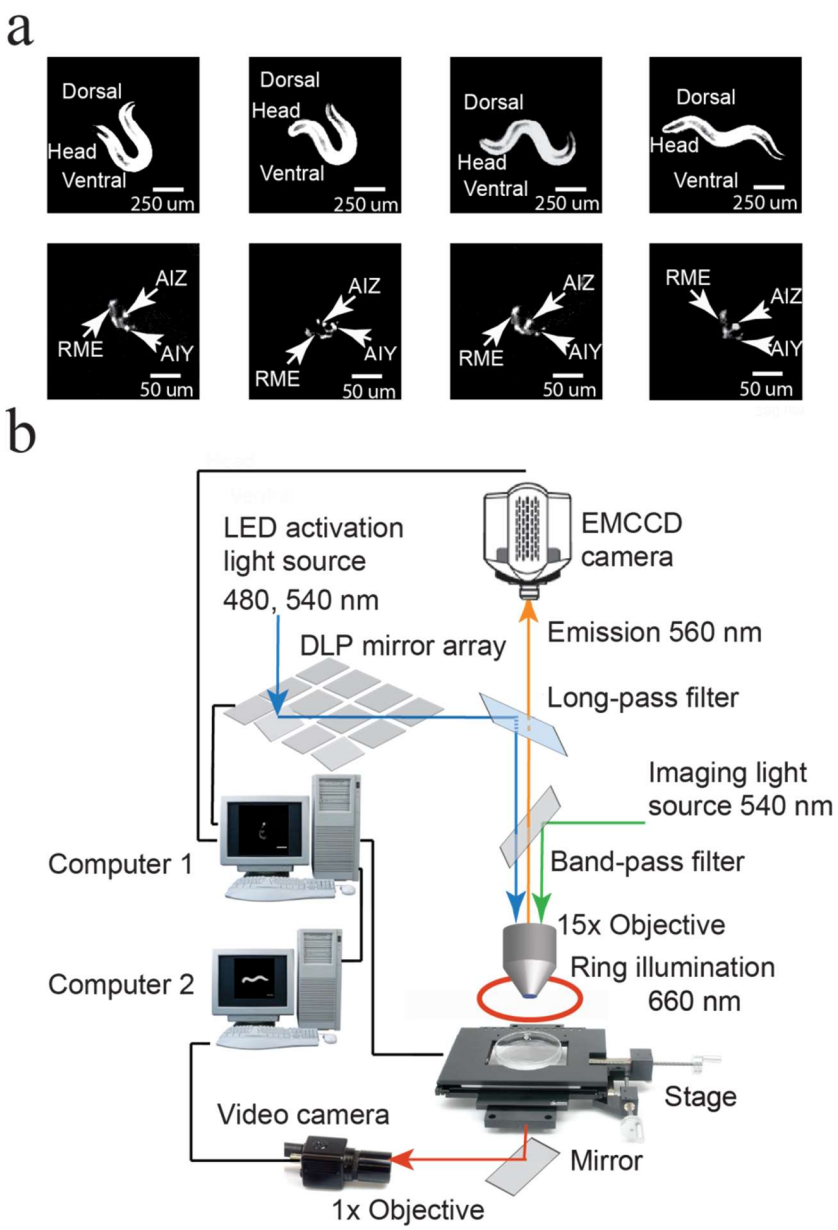

Figure 2.3: Setup for closed-loop single neuron stimulation. a, An animal expressing ChR2 and mKO in neurons AIY, AIZ and RME is shown (*ser-2prom2::ChR2; ser-2prom2::mKO*) The relative positions of neurons AIY, AIZ, and RME changed as the animal crawled (left: 1x dark field image; right: corresponding 15x fluorescence image of the neurons AIY, AIZ and RME). **b**, Setup for closed-loop single neuron stimulation (see 2.3 Method section).

Using this setup, we first tested how stimulating the interneurons AIY and AIB affected locomotory behavior. Both neuron pairs receive chemical synapses from the AWC sensory neurons that detect isoamyl alcohol[8] and showed calcium activity when animals were stimulated with this chemoattractant[9]. Asymmetric excitation of AIY with light in animals that expressed ChR2 only in AIY (under the promoter *ttx-3*) caused the animal to turn in the direction in which the head was bent when AIY were excited (Figure 2.4a). We validated our setup by reproducing these results in animals that expressed ChR2 in AIY alone and fluorescence protein monomeric Kusabira-Orange (mKO) in neurons AIY, AIZ and RME. Asymmetric stimulation of AIY in animals expressing ChR2 in AIY, AIZ and RME (*ser-2prom2*) showed the same results (Figure 2.4b-d). Consistently, inhibiting the activity in AIY asymmetrically (*pttx-3::Arch*) caused the animal turn in the opposite direction in which the head was bent when AIY were inhibited (Figure 2.4e). Symmetric excitation and inhibition of AIY decreased and increased the reversal frequency respectively, but did not cause turning (Figure 2.4f).

Both asymmetric and symmetric excitation or inhibition of AIB in AIB::*ChR2* and AIB::*Arch* animals (*npr-9* promoter) affected the reversal frequency of the animal but did not produce any gradual turning (Figure 2.4e-f). We could thus control the two locomotory behaviors crucial for chemotaxis, gradual turns and reversal frequency, by driving different patterns of activity in AIY alone.

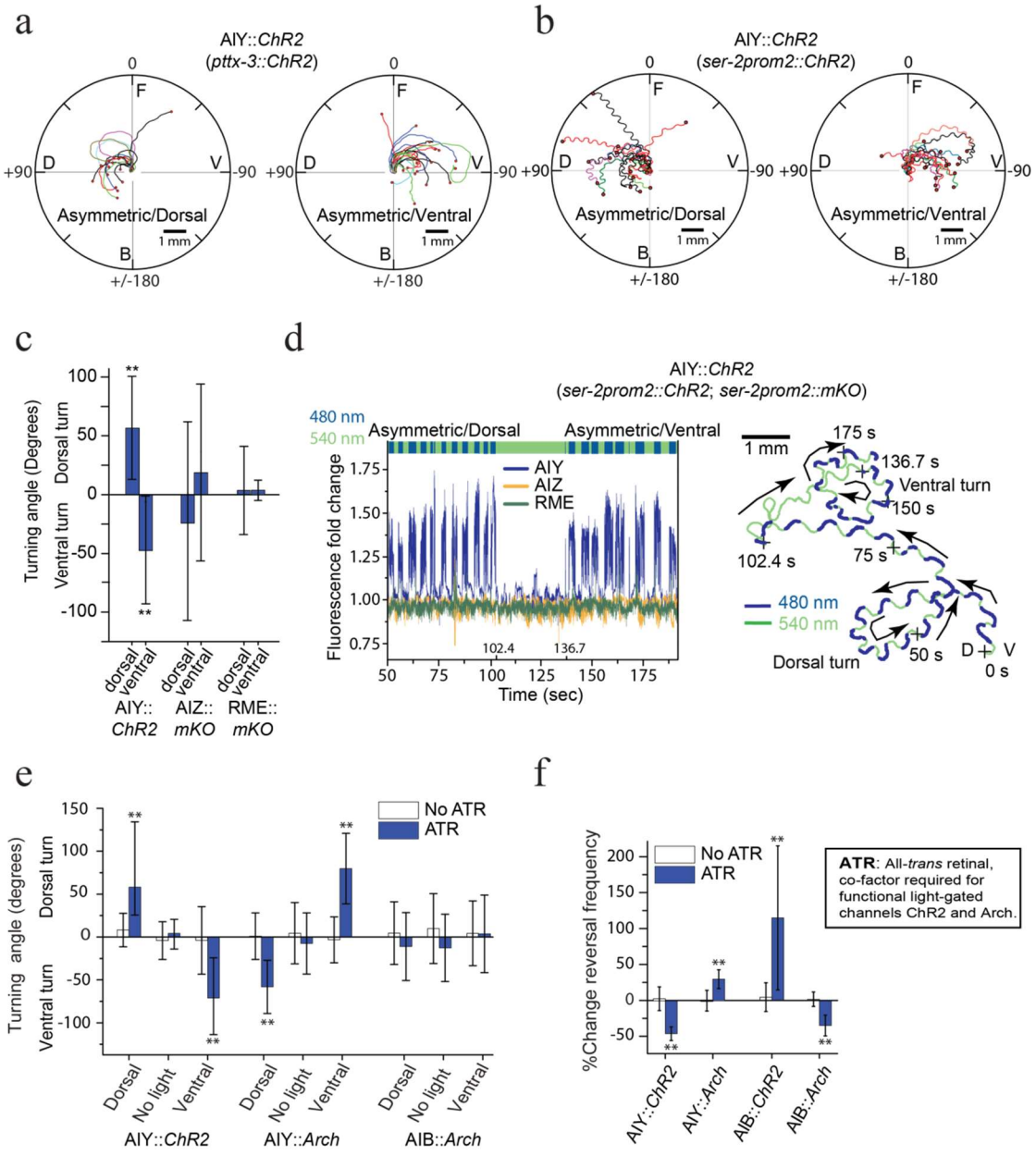

Figure 2.4: Asymmetric and symmetric excitation of AIY control gradual turning and reversal frequency. a, Sample trajectories of center of mass of animals upon dorsal or ventral asymmetric excitation of AIY (n=10, *pttx-3::ChR2*). **b,** Sample trajectories of nose tip of animals upon dorsal (left) or ventral (right) asymmetric excitation of AIY (n=10, *ser-2prom2::ChR2*). **c**, Turning angle of animals upon asymmetric stimulation of AIY::*ChR2* (n=5), AIZ::*mKO* (n=5) and RME::*mKO* (n=5). Dorsal: asymmetric dorsal stimulation. Ventral: asymmetric ventral stimulation. **, $p<0.05$, two-sample t-test. **d**, An animal co-expressing ChR2 and mKO in AIY, AIZ and RME (*ser-2prom2::ChR2; ser-2prom2::mKO*) exposed to asymmetric stimulation of AIY::*ChR2*. Time series plot of mKO fluorescence fold change (left) in AIY (blue line), AIZ (yellow), and RME (green) upon asymmetric AIY stimulation from t=50s onwards. AIY showed significant fluorescence fold change when 480nm light was focused on them but not otherwise. AIZ

(Figure 2.4 continued) and RME did not show any increase in intensity. Before 102.4s, AIY experienced asymmetric dorsal stimulation (480 nm) and from 136.7s onwards AIY experienced asymmetric ventral stimulation. The trajectory of the animal (right) shows that asymmetric dorsal stimulation led to a dorsal turn (from 0s to 102.4s) and ventral stimulation to ventral turn (t = 136.7s onwards) (blue: high power 480 nm illumination excites ChR2 (4 mW/mm^2); green: low power 540 nm illumination that does not excite ChR2 (0.1 mW/mm^2) used for imaging. **e,** Turning angle of animals upon asymmetric stimulation of AIY::*ChR2* (n=10), AIY::*Arch* (n=10) and AIB::*Arch* (n=7). No ATR: Control without all-*trans* retinal (ATR). **f,** Reversal frequencies upon symmetric stimulation of AIY::*ChR2* (n=10), AIY::*Arch* (n=19), AIB::*ChR2* (n=14), and AIB::*Arch* (n=11) (**, $p<0.05$, two-sample t-test).

2.2.4. Asymmetric excitation of AIY modulates the head bending angle to cause turning

Turning is initiated by a larger head-bending angle in one direction[18,19]. When we forced the animal to turn by asymmetrically stimulating AIY (*pttx-3::ChR2*), the head-bending angle in the direction of the turn increased (Figure 2.5), suggesting that asymmetric activation of AIY controlled head bending through head motor neurons to cause gradual turning. AIY are most directly connected to the head muscles through the interneurons AIZ which synapse onto the head motor neurons SMB and RME[8]. AIZ neurons have been implied to play a role in gradual turns by laser ablation[20]. Ablations of SMB and RME change the head-bending angle during crawling and exhibit loopy behavior[7].

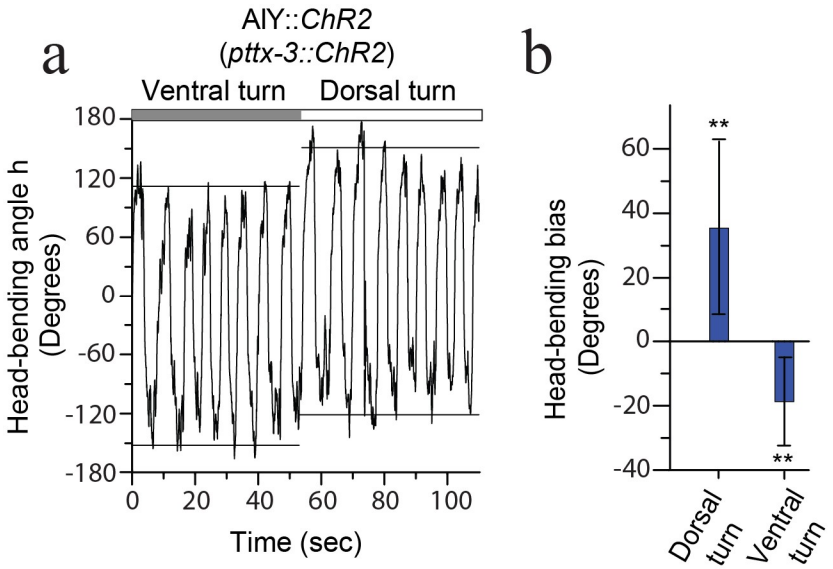

Figure 2.5: Asymmetric AIY excitation modulates the head-bending angle to cause turning. a, Representative head-bending angle (horizontal lines: means of maximum and minimum *h* during each full head swing) of an *AIY::ChR2* animal forced to first turn ventrally and then dorsally (positive: dorsal, negative: ventral). **b,** Histogram of head-bending angle bias (max(*h*)+min(*h*)) during dorsal and ventral turn caused by asymmetric AIY excitation (n=5).

When we specifically excited AIZ::*ChR2* (*ser-2prom2::ChR2*), SMB::*ChR2* (*podr-2(18)::ChR2*), or RME::*ChR2* (*ser-2prom2::ChR2)* asymmetrically using our setup, the animals turned (Figure 2.6a). These results in conjunction with those from asymmetric optical stimulation of the isoamyl alcohol sensing neuron AWC^{ON}, show that asymmetric stimulation of the sequence of anatomically connected neurons from AWC^{ON}, through the interneurons AIY, AIZ to the head motor neurons SMB and RME (Figure 2.6b) all cause turning. These set of neurons thus sense and respond to the component of the sensory signal that oscillates asymmetrically and in synchrony with head movement to control head bending and turning.

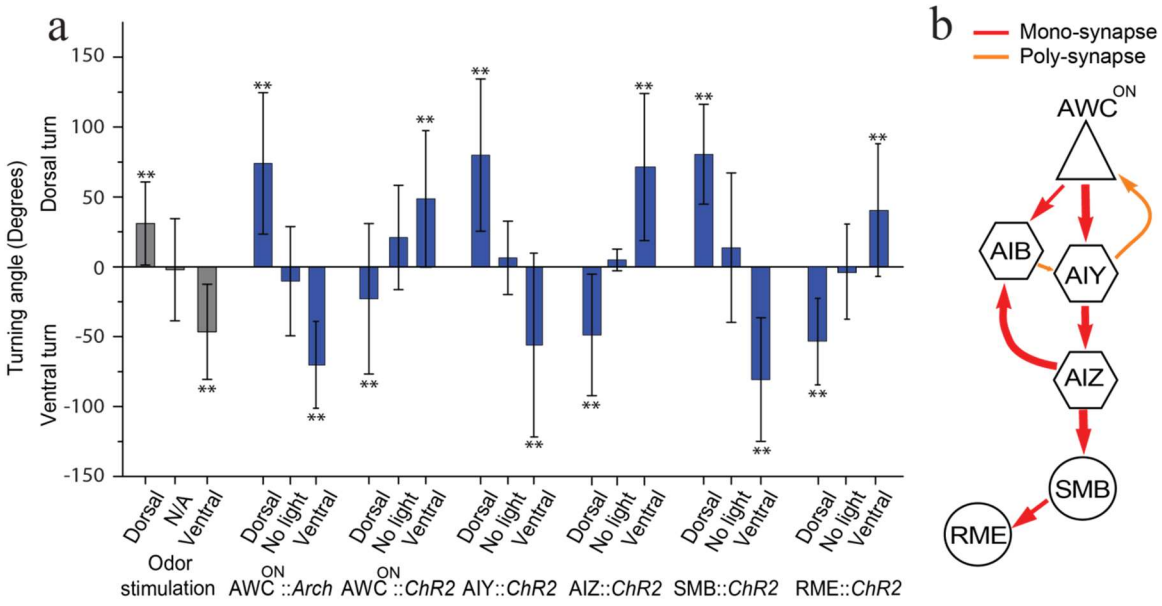

Figure 2.6: Asymmetric stimulation of AWCON and its anatomically connected neurons cause turning. a, Turning angle upon asymmetric stimulation with odor (n=10) and optically of AWC^{ON}::*Arch* (n=10), AWC^{ON}::*ChR2* (n=9), AIY::*ChR2* (n=10), AIZ::*ChR2* (n=5), SMB::*ChR2* (n=5), and RME::*ChR2* (n=5). Dorsal: asymmetric dorsal stimulation; no light: unstimulated; ventral: asymmetric ventral stimulation (**, $p<0.05$, two-sample t-test). **b,** The monadic (red) and polyadic (orange) synapses between AWC^{ON}, AIY, AIB, AIZ, SMB and RME (thickness: proportional to synapse number). Triangle: sensory neuron; hexagon: interneuron; circle: motor neuron.

2.2.5. Controlling AIY activity is sufficient to evoke chemotactic behavior

Since different patterns of activity in AIY are sufficient to control both the frequency of reversals and turning, we tested if controlling AIY activity alone was sufficient to coordinate reversal frequency and turning to evoke chemotactic behavior. To do so, we measured the locomotory behavior of animals in a fixed spatial light gradient that directly excited AIY::*ChR2* (Figure 2.7a). The animals were unable to track the gradient direction (Figure 2.7b).

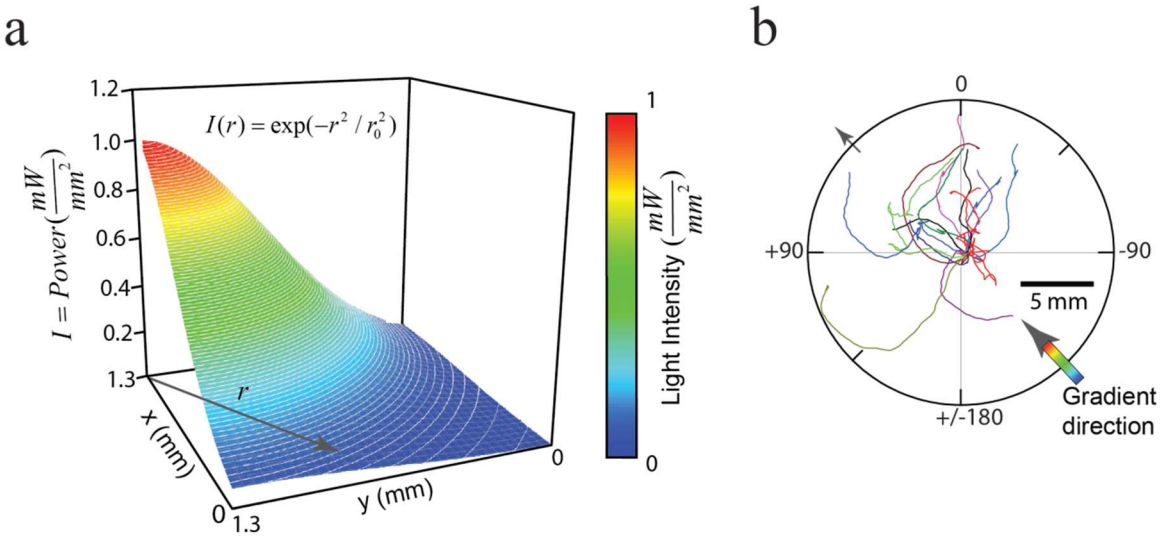

Figure 2.7: Fixed light gradient cannot elicit chemotactic behavior. a, The profile of the light gradient $I(r) = \exp(-r^2 / r_0^2)$, from 0 to 1 mW/mm^2 (pseudocolor) across 1.3 mm, where r is the distance from the peak of the gradient and r_0 = 0.8 mm. **b,** Trajectories of AIY::*ChR2* animals (n=10) moving in a fixed spatial light gradient direction at 45 degrees (arrow direction) could not stably track the gradient direction.

AIY's somas and processes are 150±25 µm behind the nose tip of an adult animal. Since the animal's speed is 150±50 µm/sec, AIY follow the position of the nose tip with approximately a one second delay. We argued that the dynamics of AIY excitation caused by the animal's movement through the gradient were not in synchrony with head bending due to this delay, preventing the animals from tracking the gradient. Therefore, we designed a virtual light gradient where the excitation light intensity on AIY depended not on the positions of AIY in space but on the position of the nose tip (Figure 2.8).

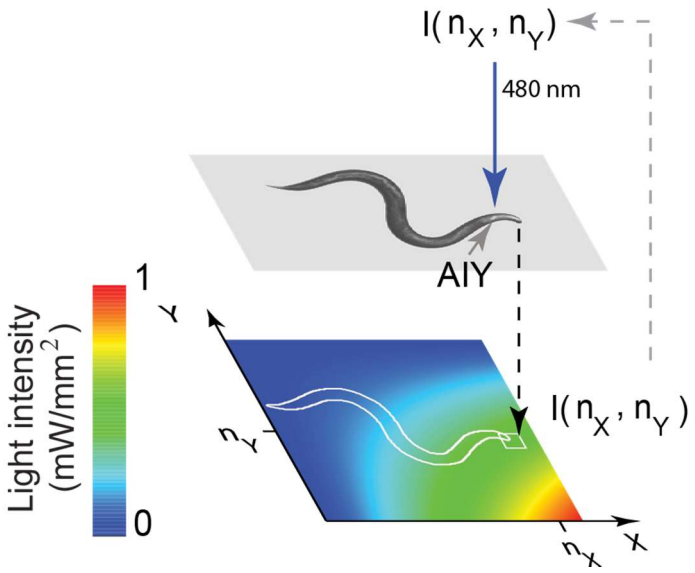

Figure 2.8: Virtual light gradient algorithm. At each time *t*, AIY*::ChR2* animals (*pttx-3::ChR2*) are stimulated with 480 nm blue light with an intensity ($I(n_x,n_y)$) of the virtual gradient at the nose-tip position (n_x,n_y).

In this setup, animals changed their locomotory direction using reversals and gradual turns to stably track the gradient direction (the fraction of the animals moving up the gradient and hence to the correct quadrant, defined as chemotaxis index = 0.94, Figure 2.9a). As with the odor profile at the nose tip, the temporal light intensity pattern that excited AIY could be written as a sum of an asymmetric ($A_I(h,t)$) and a symmetric ($S_I(h,t)$) component. When the animal's locomotory direction was not along the direction of the light gradient, the magnitude of $A_I(h,t)$ over each head swing, $|A| = \sqrt{\langle A^2{}_I(h,t) \rangle}$, was larger, exciting AIY asymmetrically to make the animal turn. As the animal oriented itself along the direction of the gradient, the magnitude of $A_I(h,t)$ continuously diminished, suppressing turns while the magnitude of $S_I(h,t)$, $|S|$, increased and suppressed reversals (Figure 2.9b-c). Thus, manipulating the dynamics of activity in just the AIY interneuron pair is sufficient to evoke chemotactic behavior. This is because the head bending and locomotion of the animal through the virtual light gradient together generate and modulate the levels of symmetric and asymmetric excitation of AIY which in turn control future locomotory behavior (Figure 2.9d).

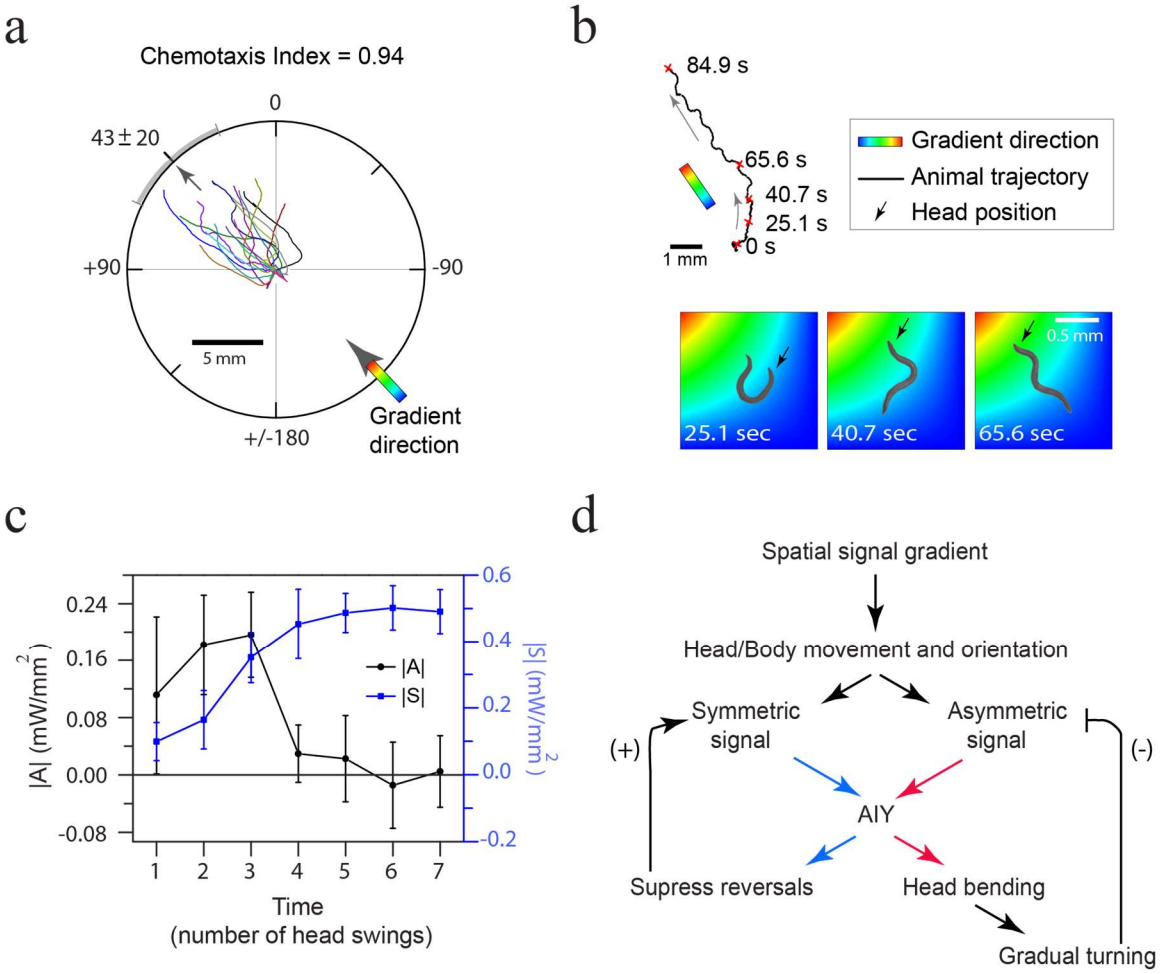

Figure 2.9: Controlling AIY activity is sufficient to evoke chemotactic behavior. a, Trajectories of AIY::*ChR2* animals moving in a virtual light gradient as in Figure 8 with a gradient direction at 45 degrees (black tick: mean direction of trajectory, grey bar: s.d., n=10). **b,** Top: A sample trajectory of an animal in (**a**). Bottom: Snapshots of the animal making a gradual turn to reorient itself to the gradient direction (pseudocolor: same as (**a**)). **c** Magnitude of A_1 (black), and S_1 (blue, right axis), over a head swing, as a function of numbers of head swings during a gradual turn (n=5, from trajectories in (**b**)). **d,** Model for chemotaxis in the virtual light gradient.

This model would predict robust chemotactic behavior in the light gradient stimulating AIY, with the symmetric and asymmetric components modulating their relative magnitudes to stably guide the animal in the correct direction. To test for robust tracking, we suddenly rotated the virtual light gradient direction by different angles and measured the animal's response. The animals followed the gradient direction as this direction was suddenly and repeatedly rotated by 180, 120 or 90 degrees (Figure 2.10).

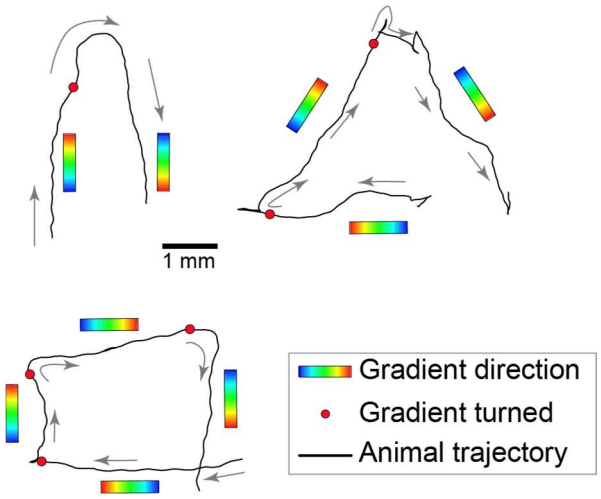

Figure 2.10: The animal track the light gradient stimulating AIY robustly. Trajectories of center of mass of animals when the gradient direction was suddenly rotated (at times when the animal reached the red dots) by 180, 120 or 90 degrees.

2.3. Discussion

Previous studies have identified neurons involved in chemotaxis by showing that defects in these neurons compromise locomotory programs and sensory modalities necessary for this behavior. Through our approach we can identify key neurons in the neural network whose dynamics are sufficient to drive chemotactic behavior and hence act as control nodes in the network. Our study leads to questions of how activity patterns stimulated in the AIY neurons during chemotaxis are disentangled by the downstream neurons to drive the different motor programs. Since many chemosensory and thermosensory neurons synapse onto AIY, the modulation of symmetric and asymmetric activity patterns in these interneurons are likely to play a central role in the different taxis behaviors of *C. elegans.* Our techniques provide avenues to eventually identify and generate neural activity patterns to control all the behaviors of this nematode.

2.4. Methods

2.4.1. Strains

Strains were grown and maintained under standard conditions[21] unless indicated otherwise. Transgenic lines with *pha-1* selection marker were grown under 24°C[22].All optical stimulation experiments were done in *lite-1* mutants to minimize the animal's sensitivity to blue light[23]. A complete strain list and information on transgenes are included in the Table 2.2.

Table 2.2: Transgenic strains, genotypes, expression patterns.

Name	Genotype	Expression
SRS167	*pha-1(e2123)* III; *lite-1(ce314)* X	N/A
SRS301	*sraEx301 [str-2p::chop-2(H134R)::TagRFP; str-2p::TagRFP; pBX];* *pha-1(e2123)*III*; lite-1(ce314)* X	AWC^{ON}, (ASI)*[24]
SRS230	*sraEx230[str-2p::Arch::TagRFP; pBX];* *pha-1(e2123)*III*; lite-1(ce314)* X	AWC^{ON}, (ASI)
SRS281	*sraEx281[ttx-3p::chop-2(H134R)::TagRFP; pBX];* *pha-1(e2123)*III*; lite-1(ce314)* X	AIY[25]
SRS279	*sraEx279[ttx-3p::Arch::TagRFP; pBX];* *pha-1(e2123)*III*; lite-1(ce314)* X	AIY
SRS291	*sraEx291[npr-9p::chop-2(H134R)::TagRFP; pBX];* *pha-1(e2123)*III*; lite-1(ce314)* X	AIB[26]
SRS278	*sraEx278[npr-9p::Arch::TagRFP; pBX];* *pha-1(e2123)*III*; lite-1(ce314)* X	AIB
SRS306	*sraEx306 [ser-2prom2::chop-2(H134R)::TagRFP; ser-2prom2::mKO; pBX];* *pha-1(e2123)*III; *lite-1(ce314)* X	AIY, AIZ, RME, DVA, BDU, [RID]**, [SIA], (PVT)[27]
SRS329	*sraEx329[odr-2(18)p::chop-2(H134R)::TagRFP; odr-2(18)p::mKO; pBX];* *pha-1(e2123)*III; *lite-1(ce314)* X	SMB, [RME], ALN, PLN, [RIG][28]
SRS392	*njIS10[glr-3p::GFP];* *sraEX112[ttx-3p::chop-2(H134R); unc-122::mCherry];* *sraEX392[ser-2prom2::mKO];* *lite-1(ce314)* X	GFP: RIA[29]; mCherry: coelomocytes, AIY; mKO: AIY, AIZ, RME, DVA, BDU, [RID]**, [SIA], (PVT)

2.4.2. Chemotaxis analysis

The animals' chemotaxis to a bacterial lawn were assayed on an open-lid, 10 cm nematode growth medium (NGM) plate incubated in room temperature overnight with 10 μL *Escherichia coli* OP50 at the center. N2 young adults were placed on the plate, 1.5 cm away from the center of the bacterial lawn. The animals' behaviors were recorded under 6x magnification by an EMCCD camera at 20Hz and analyzed by customized LabView scripts.

2.4.3. Odor stimulation setup

An N2 young adult was placed on an open-lid, food-free, 10 cm NGM plate for at least 1 minute. An electric valve (Figure 2.2a) was used to determine whether the air (100 sccm) was bubbled through water or 10-3 M isoamyl alcohol based on the posture of the freely moving animal. The images were recorded under 6x magnification by an EMCCD camera at 20 Hz and analyzed by customized LabView scripts.

2.4.4. Single neuron stimulation setup

L4 animals were transferred to a new NGM plate with a thin layer of *E. coli OP50*, containing 100 μM ATR (all-trans retinal, the co-factor required for functional light-gated ion channels) if required, 24 hours before experiments in room temperature. An animal then was placed on an open-lid, food-free, 6 cm NGM plate for at least 1 minute. Dark-field 660 nm illumination was used to visualize the posture of the animal under 1x magnification by a video camera at 20 Hz (Figure 2.3b, computer 2). Low-power 540 nm (0.1 mW/mm2) epifluorescent illumination was used to visualize the neurons co-expressing light-gated ion channels and monomeric Kusabira-Orange (mKO)[30] at 15x by an EMCCD camera at 40 Hz (computer 1). Image thresholding and particle detection were used as the image processing algorithms to identify the mKO-tagged neurons. As the animal swung its head, the neurons in the field rotated and changed their positions. To offset the rotation effect, positions of the neurons were measured using the principle axis and the distance from the center of mass of the processed image. The processed images were then used to track the animal and to position the DLP mirrors to deliver light (4 mW/mm^2, 480 or 540 nm) on the neurons of interest with any desired temporal patterns to excite or inhibit the activity of the neurons. Feedback between motorized stage, DLP

mirrors and image processing software was operated at 40 frames/sec to achieve a 5 μm spatial resolution of excitation on a freely moving animal. The images were processed, recorded, and analyzed by customized LabView scripts.

2.4.5. Reversal Frequency

L4 animals were transferred to a new NGM plate with a thin layer of *E. coli* OP50, containing 100 μM ATR if required, 24 hours before experiments in room temperature. A 6 cm copper ring was placed in an open-lid, food-free, 10 cm NGM plate immediately before experiments to keep the animals in the field of view. Young adults then were transferred to the assay plate for 1 minute before the experiment started. The desired wavelength of light (1 mW/mm^2, 480 nm or 540 nm) was delivered in alternate 3-minute intervals for 1 hour using customized LabView scripts. The experiments were recorded by a video camera at 20 Hz. Reversal frequency was calculated from pirouettes determined by an automated worm tracker (http://wormsense.stanford.edu/tracker)[31].

2.4.6. Virtual gradient setup

An AIY::*ChR2* animal was placed on an open-lid, food-free, 10 cm NGM plate for at least 1 minute before starting the experiment. A virtual-gradient of light, $I(r) = \exp\left(-r^2 / r_0^2\right)$, from 0 to 1 mW/mm^2 over 1.3 mm, where r_0=0.8 mm, was defined in an x-y coordinate system tied to the center of mass of the animal which was always at the center of the gradient profile (0.65 mm, 0.65 mm). The virtual light gradient moved with the center of mass of the animal but at a fixed orientation. At each time t, the coordinates of the nose tip were identified to calculate the corresponding intensity of light $I(n_x, n_y)$ (Figure 2.8). The animal was then illuminated with blue (480 nm) light at

intensity $I(n_x, n_y)$, and thus, AIY instantaneously experienced the intensity of light at the nose tip.

2.4.7. Molecular biology

Arch::*EGFP* was cloned into Fire lab vector kit plasmid *pPD96.52* (ligation number L2534, Addgene plasmid 1608). *Chop-2(H134R)::TagRFP* was obtained by swapping *TagRFP* with *YFP* in the previously cloned *chop-2(H134R)::YFP*. *Arch::TagRFP* and *Arch::mKO* were obtained respectively by swapping *TagRFP* or *mKO* with *EGFP* in *Arch::EGFP*. *TagRFP* and *GCaMP-3* were codon-optimized for *C. elegans* (*de novo* synthesized by GenScript) whereas others were optimized for mammalian cells. We amplified 2kb *str-2p*, 1kb *ttx-3p,* 3kb *npr-9p*, 4.5kb *ser-2prom2*, and 2.4kb *odr-2(18)p* by PCR from *C. elegans* genomic DNA. All the promoters were then fused with desired light-gated ion channels by PCR fusion.

2.5. Acknowledgements

We thank John Dowling, Shawn Lockery, Jeff Lichtman, Kathryn McCormick, Andrew Murray, Erin O'Shea, Alex Schier, Bodo Stern and members of the Ramanathan lab for discussions and comments, Human Frontier Science Program (HFSP) Postdoctoral Fellowship (A.K.), NSF Graduate Fellowship (CH.S.), NSF Career Award, Pew Scholar, Klingenstein and the NIH Pioneer Awards (S.R.) for support.

References

1. Kazushi Yoshida_Yuichi Iino_J Neurosci_2009_Parallel use of two behavioral mechanisms for chemotaxis in caenorhabditis elegans_S3.pdf.

2. Pierce-Shimomura, J. T., Morse, T. M. & Lockery, S. R. The fundamental role of pirouettes in Caenorhabditis elegans chemotaxis. *The Journal of neuroscience : the official journal of the Society for Neuroscience* **19,** 9557–69 (1999).

3. Ward, S. Chemotaxis by the Nematode Caenorhabditis elegans: Identification of Attractants and Analysis of the Response by Use of Mutants. *Proceedings of the National Academy of Sciences* **70,** 817–821 (1973).

4. Izquierdo, E. J. & Lockery, S. R. Evolution and Analysis of Minimal Neural Circuits for Klinotaxis in Caenorhabditis elegans. *Science* **30,** 12908 –12917 (2010).

5. Tsalik, E. L. & Hobert, O. Functional mapping of neurons that control locomotory behavior in Caenorhabditis elegans. *Journal of neurobiology* **56,** 178–97 (2003).

6. Wakabayashi, T., Kitagawa, I. & Shingai, R. Neurons regulating the duration of forward locomotion in Caenorhabditis elegans. *Neuroscience research* **50,** 103–11 (2004).

7. Gray, J. M., Hill, J. J. & Bargmann, C. I. A circuit for navigation in Caenorhabditis elegans. *Proceedings of the National Academy of Sciences of the United States of America* **102,** 3184–91 (2005).

8. White, J., Southgate, E., Thomson, J. N. & Brenner, S. The structure of the nervous system of the nematode Caenorhabditis elegans. *Phil. Trans. Royahl Soc. Lond. B* **314,** 1–340 (1986).

9. Chalasani, S. H. *et al.* Dissecting a circuit for olfactory behaviour in Caenorhabditis elegans. *Nature* **450,** 63–70 (2007).

10. Leifer, A. M., Fang-Yen, C., Gershow, M., Alkema, M. J. & Samuel, A. D. T. Optogenetic manipulation of neural activity in freely moving Caenorhabditis elegans. *Nature Methods* (2011). doi:10.1038/nmeth.1554

11. Chalfie, M. *et al.* The neural circuit for touch sensitivity in Caenorhabditis elegans. *The Journal of neuroscience : the official journal of the Society for Neuroscience* **5,** 956–64 (1985).

12. Boyden, E. S., Zhang, F., Bamberg, E., Nagel, G. & Deisseroth, K. Millisecond-timescale, genetically targeted optical control of neural activity. *Nature neuroscience* **8,** 1263–8 (2005).

13. Nagel, G. *et al.* Light activation of channelrhodopsin-2 in excitable cells of Caenorhabditis elegans triggers rapid behavioral responses. *Current biology : CB* **15,** 2279–84 (2005).

14. Chow, B. Y. *et al.* High-performance genetically targetable optical neural silencing by light-driven proton pumps. *Nature* **463,** 98–102 (2010).

15. Okazaki, A., Sudo, Y. & Takagi, S. Optical silencing of C. elegans cells with arch proton pump. *PloS one* **7,** e35370 (2012).

16. Guo, Z. V, Hart, A. C. & Ramanathan, S. Optical interrogation of neural circuits in Caenorhabditis elegans. *Nature methods* **6,** 891–6 (2009).

17. Stirman, J. N. *et al.* Real-time multimodal optical control of neurons and muscles in freely behaving Caenorhabditis elegans. *Nature methods* (2011). doi:10.1038/nmeth.1555

18. Kim, D., Park, S., Mahadevan, L. & Shin, J. H. The shallow turn of a worm. *Journal of Experimental Biology* 1554–1559 (2011). doi:10.1242/jeb.052092

19. Lockery, S. R. The computational worm: spatial orientation and its neuronal basis in C. elegans. *Current opinion in neurobiology* (2011). doi:10.1016/j.conb.2011.06.009

20. Iino, Y. & Yoshida, K. Parallel use of two behavioral mechanisms for chemotaxis in Caenorhabditis elegans. *The Journal of neuroscience : the official journal of the Society for Neuroscience* **29,** 5370–80 (2009).

21. Brenner, S. & Ls, D. P. F. J. The genetics of behaviour. *Prospects* **29,** 269–271

22. Granato, M., Schnabel, H., Schnabel, R., Biochemie, M. & A, A. K. selectable marker for transfer in C . elegans. *Science* **22,** 1762–1763 (1994).

23. Edwards, S. L. *et al.* A novel molecular solution for ultraviolet light detection in Caenorhabditis elegans. *PLoS biology* **6,** e198 (2008).

24. Peckol, E. L., Troemel, E. R. & Bargmann, C. I. Sensory experience and sensory activity regulate chemosensory receptor gene expression in Caenorhabditis elegans. *Proceedings of the National Academy of Sciences of the United States of America* **98,** 11032–8 (2001).

25. Hobert, O., D'Alberti, T., Liu, Y. & Ruvkun, G. Control of neural development and function in a thermoregulatory network by the LIM homeobox gene lin-11. *The Journal of neuroscience : the official journal of the Society for Neuroscience* **18,** 2084–96 (1998).

26. Bendena, W. G. *et al.* A Caenorhabditis elegans allatostatin/galanin-like receptor NPR-9 inhibits local search behavior in response to feeding cues. *Proceedings of*

the National Academy of Sciences of the United States of America **105,** 1339–42 (2008).

27. Tsalik, E. LIM homeobox gene-dependent expression of biogenic amine receptors in restricted regions of the C. elegans nervous system. *Developmental Biology* **263,** 81–102 (2003).

28. Chou, J. H., Bargmann, C. I. & Sengupta, P. The Caenorhabditis elegans odr-2 gene encodes a novel Ly-6-related protein required for olfaction. *Genetics* **157,** 211–24 (2001).

29. Brockie, P. J., Mellem, J. E., Hills, T., Madsen, D. M. & Maricq, a V. The C. elegans glutamate receptor subunit NMR-1 is required for slow NMDA-activated currents that regulate reversal frequency during locomotion. *Neuron* **31,** 617–30 (2001).

30. Karasawa, S., Araki, T., Nagai, T., Mizuno, H. & Miyawaki, A. Cyan-emitting and orange-emitting fluorescent proteins as a donor / acceptor. *Society* **312,** 307–312 (2004).

31. Ramot, D., Johnson, B. E., Berry, T. L., Carnell, L. & Goodman, M. B. The Parallel Worm Tracker: a platform for measuring average speed and drug-induced paralysis in nematodes. *PloS one* **3,** e2208 (2008).

Chapter 3. Function and activity patterns of AIY and neurons downstream of AIY

[Authors: Ching-Han Shen, Jeffrey Lee, Askin Kocabas, Abdullah Yonar, and Sharad Ramanathan. C.–H.S. made transgenic lines, planned and performed experiments, and developed analysis. J.L. built the optical setup, planned experiments and developed analysis related to section 3.2.3. A.K. designed and built the optical setup. A.Y. performed experiments related to Figure 3.3, S.R. planned experiments and helped develop analysis.]

Abstract

Chapter 2 shows how controlling the activity of AIY can coordinate gradual turning and reversals to evoke chemotactic behavior in *C. elegans.* However, we still do not know how AIY transmits environmental information to its downstream neurons to ultimately control behavior. We used the GCaMP imaging system developed in the laboratory to record the activity of AIY and three out of four downstream interneurons (AIZ, RIA, and RIM), as well as the animal's movement, in response to odor. We found that AIY and RIA are positively correlated with the presence of odor, whereas AIZ and RIM are negatively correlated with the presence of odor. We then used optogenetic tools to control the activity of the three neurons to study the functions of them. We observed that interneurons AIZ and RIA control gradual turning and interneurons RIM control reversals. Combined with evidence from preexisting literature, we proposed possible functional connections between neurons involved in chemotaxis. The results can guide

what experiments will be needed to fully understand the flow of information from environmental stimuli to behavioral control.

3.1. Introduction

Chapter 2 describes how we used optogenetics and new optical tools to directly perturb neural activity in freely moving animals to evoke chemotactic behavior. We discovered that controlling the activity in just one pair of interneurons (AIY) is sufficient to evoke chemotactic behavior[1]. Since many sensory neurons directly connect to AIY[2], together with our finding, it suggests that AIY can integrate signals from sensory neurons and can coordinate its downstream neurons to modulate the animal's locomotion to perform chemotaxis.

However, we still do not know how the information from environmental stimuli transmits from AIY to downstream neurons to control behaviors. To address this question, we need to know: (1) what naturally occurring activity patterns in AIY are; (2) how AIY and the downstream interneurons respond to environmental stimuli; (3) what behaviors are controlled by interneurons downstream of AIY.

To answer these questions, it is necessary to image activities in neurons in freely moving animals, which presents technical challenges. Previous studies have tracked animals for only short periods of time, which is insufficient to study the correlation between neural activities and the animal's behaviors[3–5]. Imaging neural activity requires tracking under high magnification and measuring calcium activity with long exposure times. Neural activity is often only observed in the 1-μm diameter processes[8] and therefore requires high magnification to resolve. Exposure of high light power on *C. elegans* can damage them and cause their locomotion to become sluggish. Therefore,

long exposure times are required to minimize the light power for illumination. However, *C. elegans* can move up to 300 μm per second, which poses two challenges: First, the animal leaves the field of view quickly under high magnification without tracking. Second, the quality of the acquired images will be very low due to motion blur. To overcome the challenges, people in the laboratory built an optical system to track the animal by using fast imaging and mechanical feedback to compensate for its movement.

Tracking at high magnification requires fast loop rates, whereas imaging calcium activity requires long exposures and slower rates. The system built in the laboratory uses two independent feedback loops to satisfy both requirements. First, the tracking feedback loop images 100 times per second to track a neuron of interest within 5 um. It compensates for the animal's movement in horizontal (x, y), vertical (z) and rotation displacement so that the animal appears stationary to the GCaMP imaging feedback loop. Second, the GCaMP imaging feedback loop operates 16 times per second to measure calcium activity in neurons of interest (Figure 3.1). These two feedback loops together allows us to track the animal and measure the GCaMP activity in neurons of interest in a freely moving animal.

In this chapter, we discussed what we learned from observing the nautrally-occuring activity patterns of AIY and of the downstream neurons, what functions the neurons downstream of AIY control, and what we need to do to further understand the system.

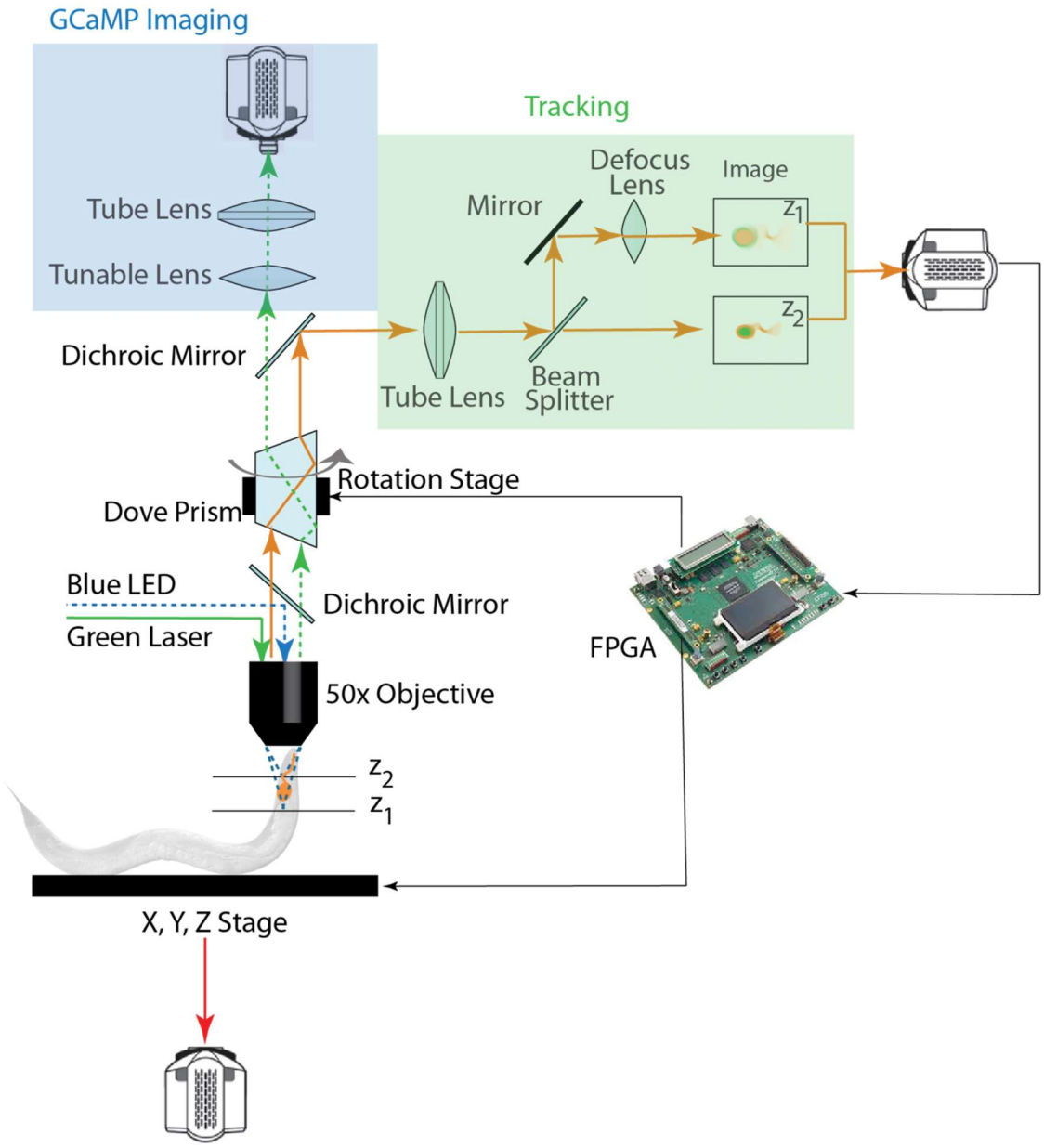

Figure 3.1: System built in the laboratory to image calcium activity in neurons in freely moving animal. Green and orange solid lines represent the light path of green laser for using a marker neuron to stably track in x, y, z and rotation. Blue and green dash lines represent the light path of blue LED for calcium imaging. Red solid line represents the light path to image the body posture of the animal. Fast tracking feedback loop allows us to image GCaMP in low light power with long exposure time. For more detail of the system, see method section 3.5.3.

3.2. Results

3.2.1. Select suitable marker neuron for the calcium imaging system built in the laboratory

Good tracking of the marker neurons in x, y, z and rotation is crucial to obtain a high quality of calcium measurement in the calcium imaging system. The marker neuron has to be a single neuron with a single process for rotation tracking. I surveyed the literature to find available promoters that can be used to express fluorescence protein in a single neuron, which narrowed down the candidate neurons to ASEL, ASER[9] and AWC^{ON}[10]. In addition, we wanted to use low light power for tracking and therefore the fluorescence protein expression in the marker neuron has to be bright. I expressed fluorescence protein, mKO (monomeric Kusabira Oranage)[11], in each of the candidate neurons. The expression of AWC^{ON}::mKO is consistently brighter than the other two candidates (data not shown) and the process of AWC^{ON} can be imaged clearly (Figure 3.2). I therefore integrated the transgenic line so that the expression of AWC^{ON}::mKO is relative stable and this line can be used to generate other lines that also express GCaMP in there.

Figure 3.2: AWC^{ON}::mKO expression is bright and the process can be seen clearly. Scale bar represents 10 μm.

Using the integrated AWC^{ON}::mKO line, I expressed EGFP (enhanced green fluorescence protein) in AIY so that people in the laboratory can validate the stability of

the calcium imaging system. During over 20 minutes of tracking, there was little photo bleaching and the intensity measured was constant with less than 20% relative standard error, which is calculated by standard deviation divided by mean (data not shown). I used the relative standard error as our error bar for measurements of relative changes in GCaMP intensity in experiments below.

3.2.2. Naturally occurring activity of AIY correlates with reversal frequency

Controlling the activity of interneurons AIY can make an animal coordinate reversal frequency and gradual turning to evoke chemotactic behavior by optogenetic stimulation. However, optogenetic perturbation pushes the activity in neurons to an extreme. It is not clear if perturbation can mimic the naturally occurring activity in neurons.

We started by measuring the calcium activity in both the soma and processes of AIY while an animal moved freely on an agar plate without food or artificial stimuli. We observed changes in the activity of both soma and processes of AIY (Figure 3.3a). The activity levels in the processes change quickly and can double within 3 seconds (Figure 3.3b). In contrast, the activity of the soma changes slowly (Figure 3.3c) and can sustain a consistent level for more than 10 minutes, which might be the reason why previous studies only reported activity changes in the processes of AIY but not in the soma of AIY[5,8].

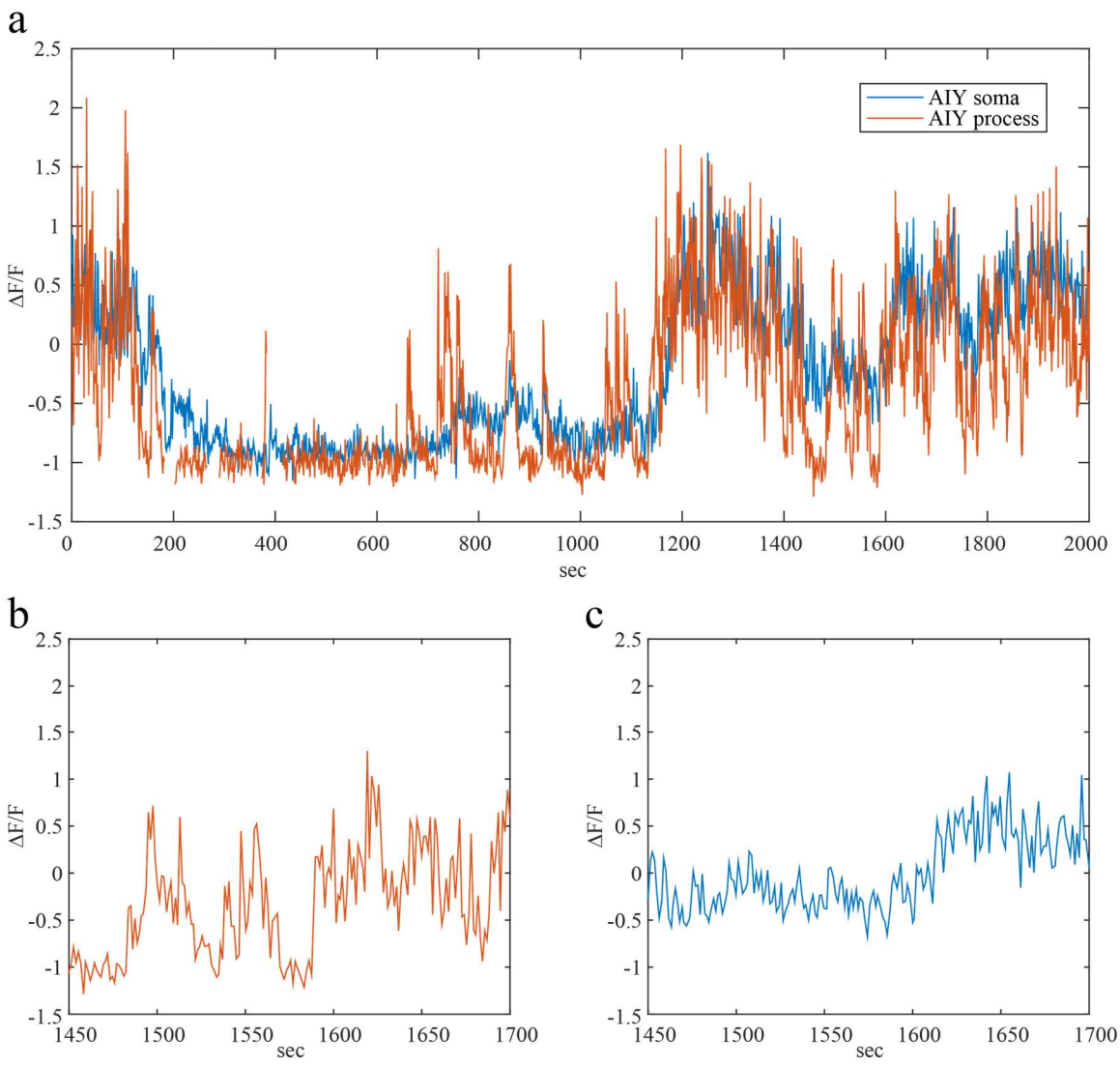

Figure 3.3: Activity of AIY changes when an animal navigates an agar plate without food or other external stimuli. a, Calcium activity of AIY soma and processes through 2000 seconds of tracking. Blue line represents the activity of AIY soma. Red line represents the activity of AIY processes. Grey area represents loss of tracking. **b-c**, The activity of AIY processes (**b**) and soma (**c**) during 1450~1700 seconds from (**a**). Activities of both AIY soma and processes change through the time course of 2000 seconds without external stimuli. Changes of activity in AIY process are faster than changes of activity in AIY soma.

We then asked if the activity changes of AIY correlate with changes in behaviors. We observed that the animal tends to reverse more often when the activity of AIY is low than when the activity of AIY is high (Figure 3.4). This result is consistent with what we found in optogenetic stimulation of AIY: Reversal frequency of an animal is low during depolarization of AIY and the reversal frequency of an animal is high during hyperpolarization of AIY (Figure 2.4).

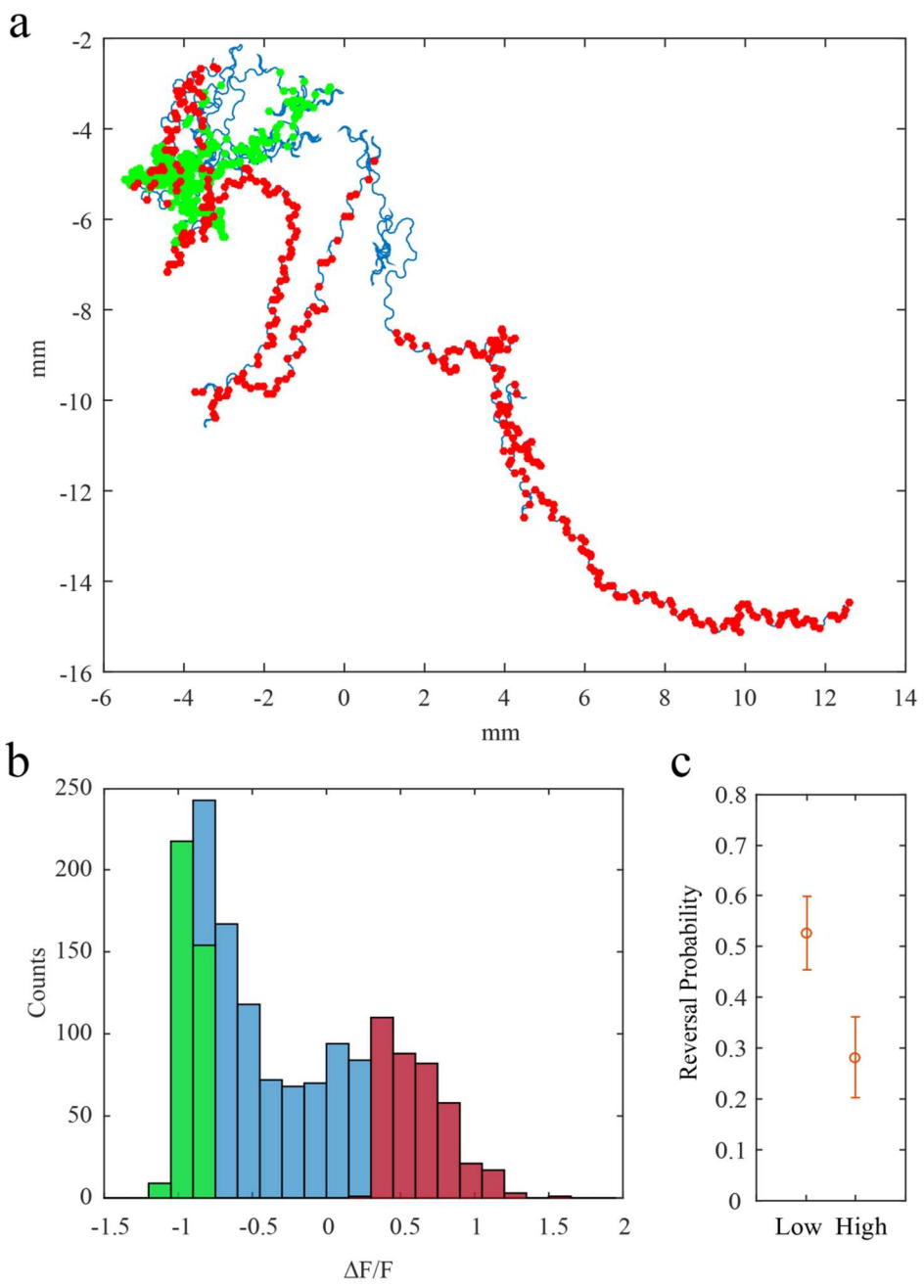

Figure 3.4: Reversal probability is lower when the activity of AIY soma is high than when the activity of AIY low. a, An example of the trajectory of the animal's head movement overlaid with low (green) and high (red) AIY soma activity. Blue line represents the trajectory of the animal's head movement in Figure 3.3. Green dots represent low AIY activity. Red dots represent high AIY activity. **b**, The histogram of AIY soma activity of the animal in (**a**). Green represents low activity of AIY soma (lower than 25th percentile of total data points). Red represents high activity of AIY soma (higher than 75th percentile of total data points). Blue represents the rest of activity of AIY soma. **c**, The reversal probability of low AIY soma activity and high AIY soma activity (n=5 independent experiments, each experiment lasted more than 20 minutes).

3.2.3. AIY and interneurons downstream of AIY respond to bacterial odor

C. elegans senses odor from bacterial lawn to perform chemotaxis. To understand how the information of bacterial odor transmits from AIY to the downstream neurons, we first asked which neurons are involved in sensing the odor. There are 4 pairs of interneurons downstream of AIY (Figure 3.5). AIY connects to AIZ, RIA and RIB through chemical synapses and to RIM through gap junctions. In this chapter, we discuss the role of the downstream neurons AIZ, RIM and RIA. Reagents for RIB are still in preparation.

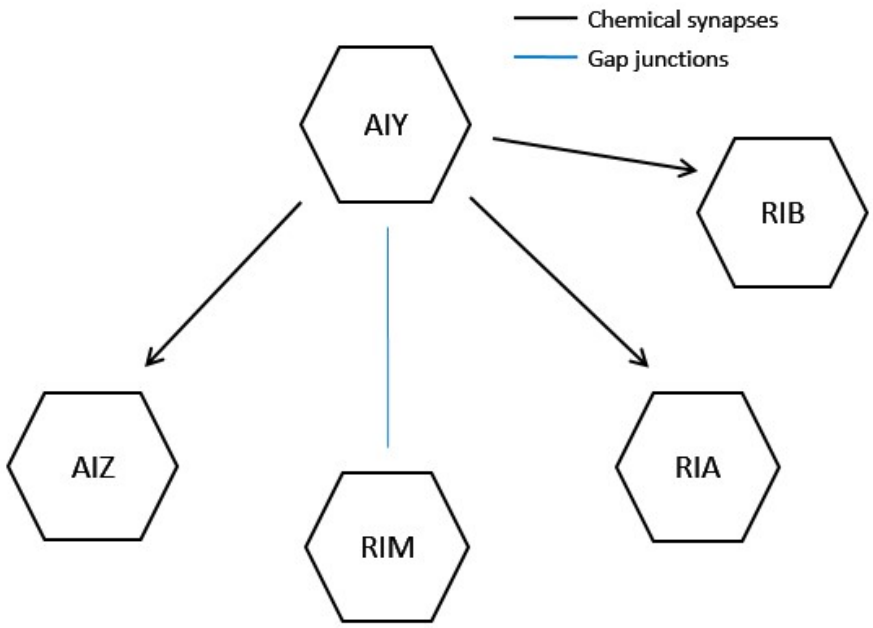

Figure 3.5: Cartoon diagram of interneurons downstream of AIY. Black arrows represent chemical synapses; blue line represents gap junctions.

I used ser-2prom2 to express GCaMP in AIZ and other neurons. In the presence of odor, AIZ showed decrease of activity; whereas in the absence of odor, AIZ showed increase of activity (Figure 3.6a). However, the naturally occurring calcium activity of AIZ also changes around the same amplitude as the changes from the effects of odor

(Figure 3.6b). As a result, it is difficult to distinguish the activity changes caused by odor versus other factors with this odor delivery method.

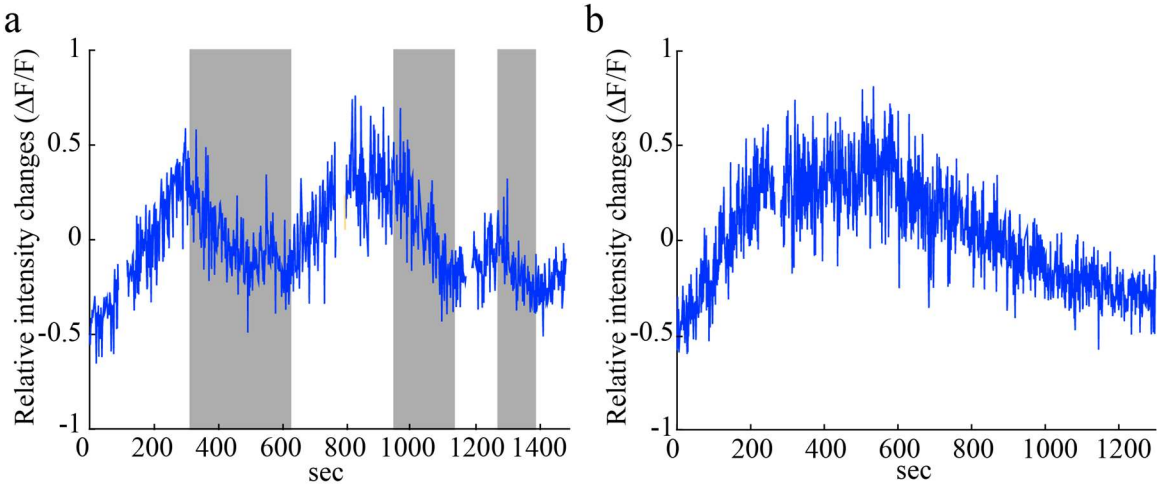

Figure 3.6: Examples of changes of calcium activity of AIZ in the presence and absence of odor. a, Calcium activity of AIZ showed decrease of activity in the presence of odor and increase of activity in the absence of odor. Blue line represents the activity of AIZ soma. Grey area represents the presence of bacterial odor. **b**, Activity of AIZ in the absence of odor. The naturally occurring calcium activity of AIZ changes around the same amplitude as the changes from the effects of odor. As a result, it is difficult to disentangle which parts of the activity changes in neurons of interest are from the effect of the addition of bacterial odors.

To address the challenge, we imposed an artificial and arbitrary periodic odor signal on the animal. We chose a period of 120 seconds because it is longer than the time scale of turning and reversals and is short enough to have many consecutive periods for quantification.

We first used this method to characterize the correlation of AIZ activity and odor signals (Figure 3.7). We quantified the correlation between the changes of calcium activity of AIZ and odor signals by Pearson's correlation coefficient. The latency was determined by identifying how much time delay of AIZ activity changes can lead to the maxima Pearson's correlation coefficient. The Pearson's correlation coefficient of the original data is at least 2~3 standard deviations away from the mean of 400 other random permutation from original data. We found that the calcium activities in AIZ are

negatively correlated with odor delivery, which is consistent with previous results with long odor delivery (Figure 3.6). This method can help us quantify the correlation between the activity of neurons and odor signals.

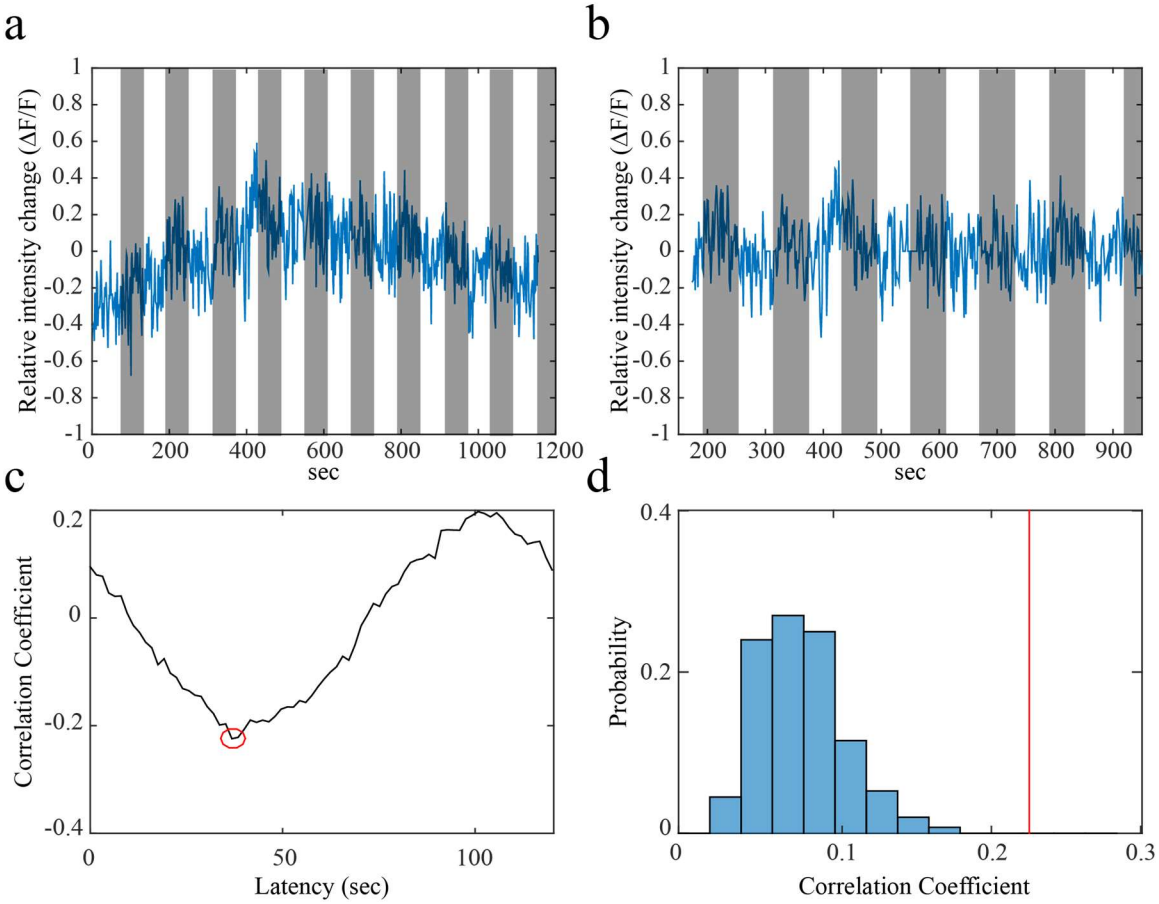

Figure 3.7: Activity of AIZ is negatively correlated with the delivery of bacterial odor. a, An example of the activity of AIZ with the presence of odors for 60 seconds and the absence of odors for 60 seconds repeatedly. Blue line represents the activity of AIZ. Grey area represents the presence of odor. **b**, The activity of AIZ in (**a**) after corrected for the baseline. The first and last 160 seconds were truncated after the correction. **c**, The Pearson's correlation coefficient calculated from (**b**) with the latency from 0 to 120 seconds. Red circle represents the maxima Pearson's correlation coefficient in the presence of odors. **d**, 400 data sets were generated by randomly permuting the activity of AIZ in (**b**). The maxima correlation coefficients within 120 second latency were then used to plot the histogram. The value from (**c**), represented by red line, is more than 2 standard deviations away from the mean of the histogram and therefore the correlation is considered statistically significant.

We used the same method to study the response of AIY, RIA and RIM to bacterial odor. There are neuron-specific promoters for all three neurons, which allowed us to resolve the processes and measured the activity of both the soma and processes. All neurons measured here responds to bacterial odor (Figure 3.8). Together, the results suggested that the activity levels of AIZ and RIM are negatively correlated with the presence of odor; whereas RIA and AIY are positively correlated with the presence of odor.

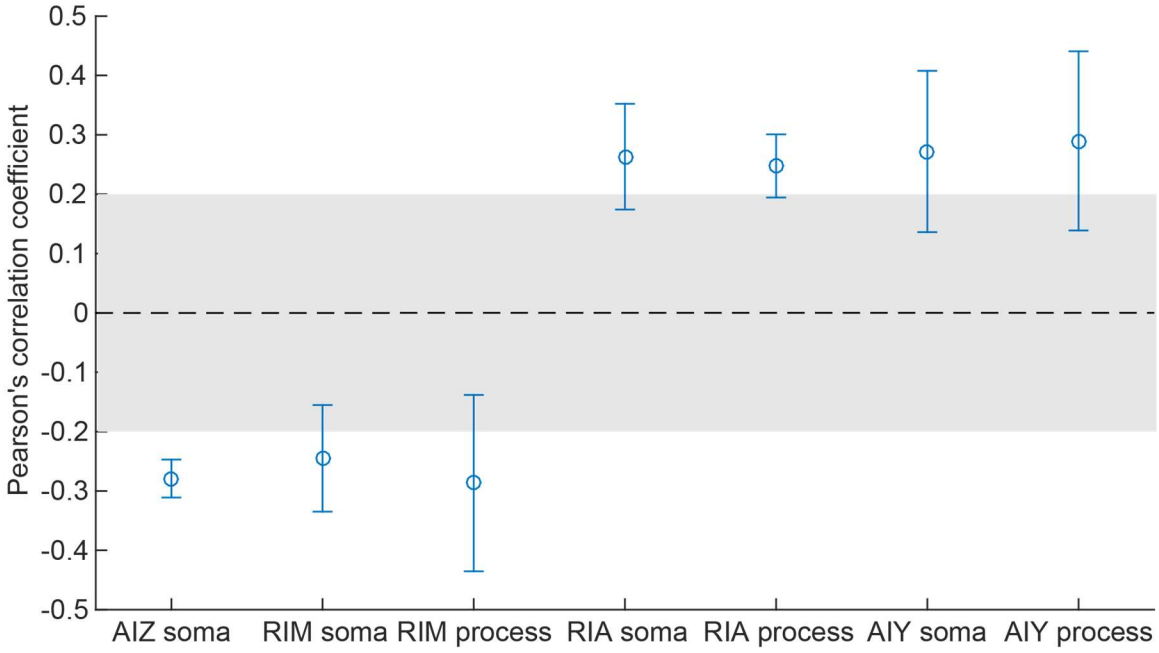

Figure 3.8: Correlation of periodic odor signals and activity of neurons downstream of AIY and AIY. Pearson's correlation coefficient of odor signals and activity of neurons. Grey area represents the correlation (-0.2~0.2) a permutated dataset might get by chance. Number of experiments: AIZ=4; RIM=4; RIA=6; AIY=9. Each experiment was at least 15 minutes long. RIA and AIY are positively correlated with the presence of odor; whereas AIZ and RIM are negatively correlated with the presence of odor.

3.2.4. Activities of AIY, RIM and RIA are correlated with reversal rate

Next we asked what behavior correlates with the changes of activity. We started by examining the correlation of reversals and activity changes of neurons. In the case of RIM, we observed that the rise and fall of RIM process activity correlates with the occurrence of reversal events (Figure 3.9). On the other hand, RIM soma activity changes more gradually and seems to coincide with reversal rate than occurrence of reversal events.

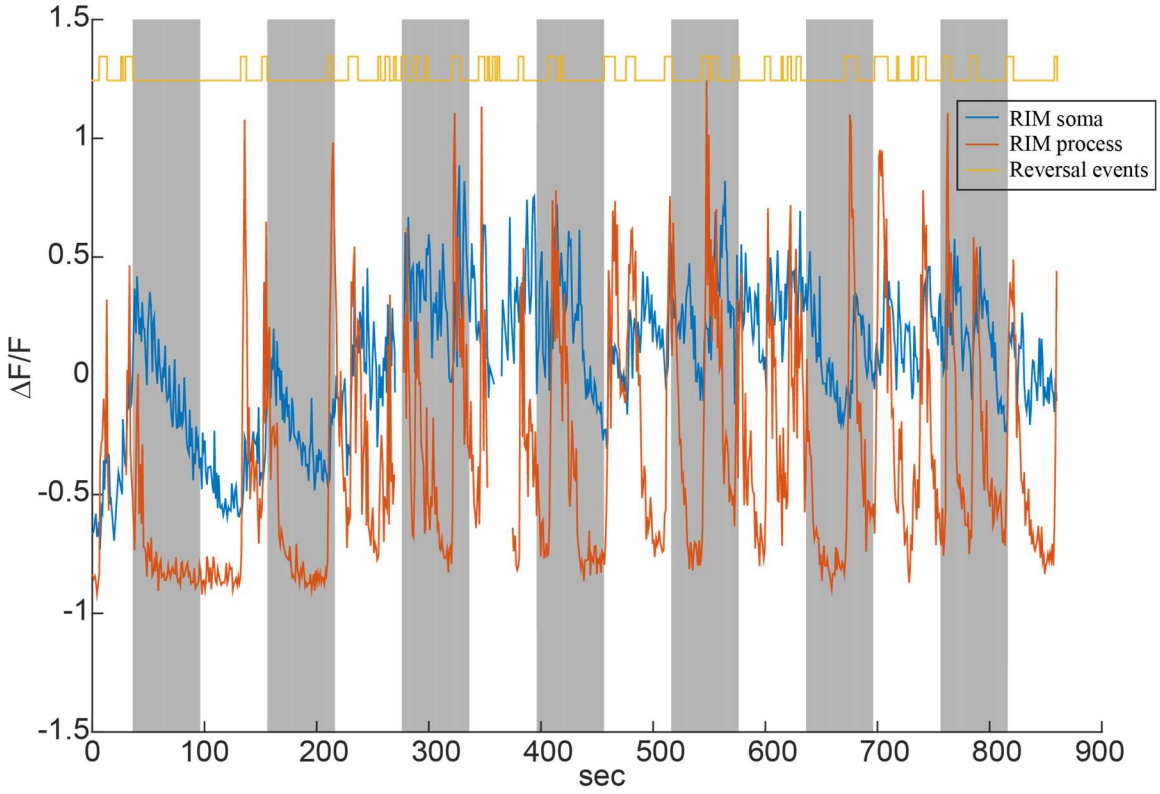

Figure 3.9: The dynamics of activities of RIM soma and processes are different. Blue: Activity of RIM soma; Red: Activity of RIM processes; Yellow: reversal events. Grey area represents the presence of bacterial odor. Activity changes of RIM soma and process are both correlated with reversal rate.

We defined a reversal event as the duration an animal reverses. Reversal rate, however, is trickier to define: the integration time of different neurons might vary and therefore we need to determine the optimal average window for every neuron. We tested

the correlation of neural activity and reversal rate with moving average windows of 3, 10, 30, 60, 100 and 150 seconds. We found that RIM soma has the highest correlation with reversal rate with moving average windows of 60 seconds; whereas the correlation of RIM process activity and reversal rate is highest with 10 seconds as the moving average window (Figure 3.10).

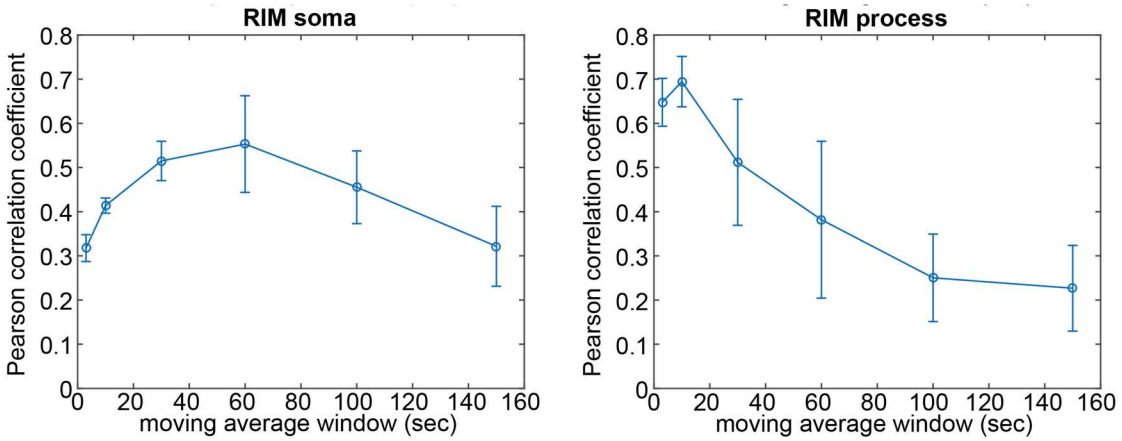

Figure 3.10: RIM soma and process have different integration time. RIM soma has the highest correlation with reversal rate with 60 seconds moving average window; whereas RIM process has the highest correlation with reversal rate with 10 seconds moving average window.

We used the same method to quantify the correlation of the activity of other neurons and reversal rate (Figure 3.11 and Figure 3.12). The results showed that AIY and RIA are negatively correlated with reversal rate, RIM is positively correlated with reversal rate, and AIZ is not correlated with reversal rate. We also noticed that the optimal moving average window is always longer in the soma than in the process. However, we do not have tools to test if this observation has biological meaning.

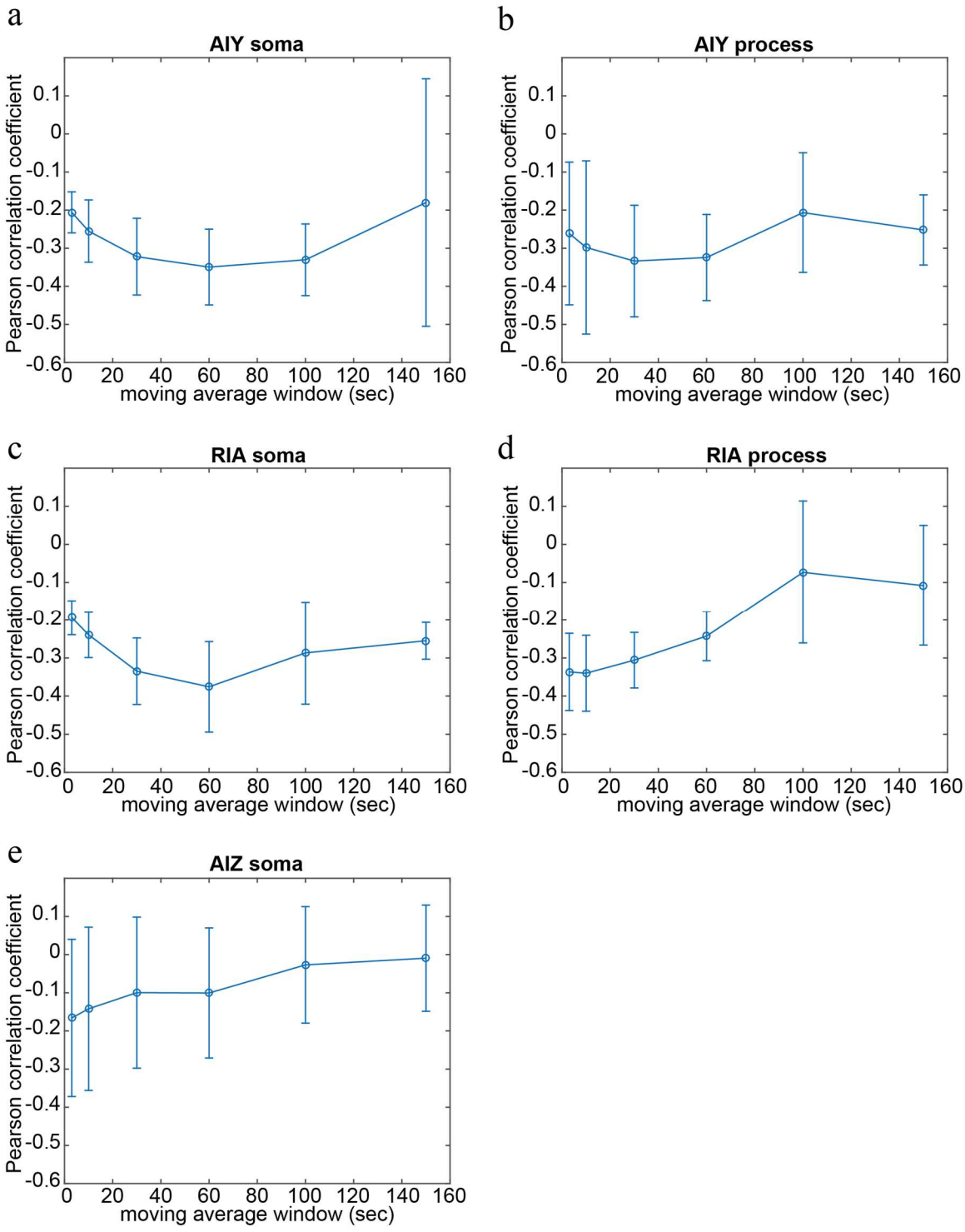

Figure 3.11: Correlation of activity of neurons and reversal rate calculated with moving average windows of 3, 10, 15, 30, 60 and 150 seconds. The figure was produced based on the same experiments in Figure 3.8.

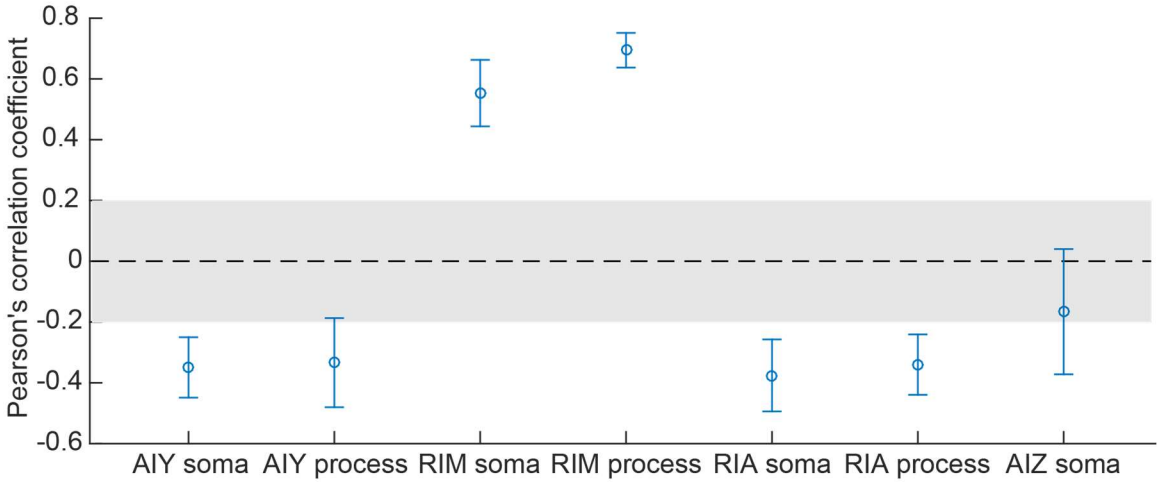

Figure 3.12: The correlation of neural activity and reversal rate. The correlation was obtained from the highest correlation in Figure 3.10 and Figure 3.11.

We also expressed express ChR2 in neurons that correlate with reversal rate and tested if they are involved in controlling reversals (Figure 3.13). Excitation of AIY leads to reversal inhibition; whereas excitation of RIM promotes reversals. The results are consistent with what we observed in calcium imaging (Figure 3.12). Excitation of RIA does not promote or inhibit reversals significantly. It is possible that RIA does not control reversals but rather only encodes information related to the animal's movement.

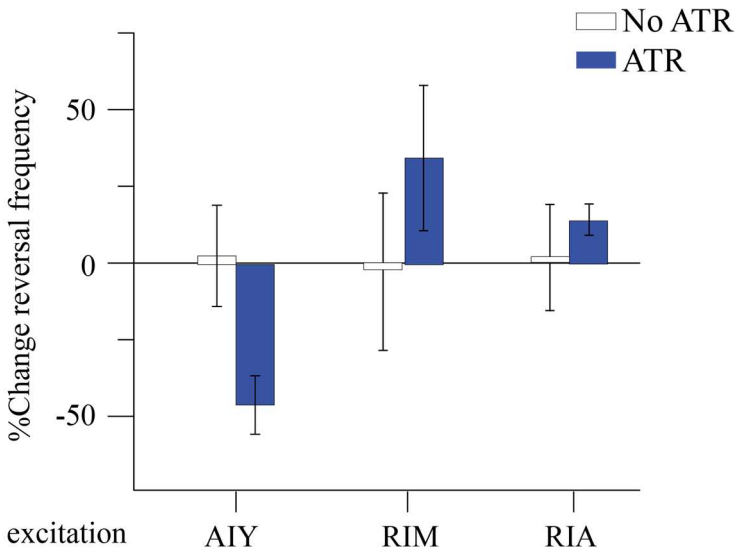

Figure 3.13: Reversal frequency upon symmetric excitation of AIY and its downstream interneurons. Reversal frequencies upon symmetric excitation of AIY::*ChR2* (n=10), RIM::*ChR2* (n=6), and RIA::*ChR2* (n=13).

3.2.5. AIZ and RIA controls gradual turning

Since AIY also controls gradual turning during chemotaxis, we next wanted to know which neurons are involved in controlling gradual turning. From Chapter 2, we showed that asymmetric excitation of AIY leads to graduate turning to the same side of the excitation (Figure 2.4); whereas asymmetric excitation of AIZ leads to graduate turning to the opposite side of the excitation (Figure 2.6, Figure 3.14).

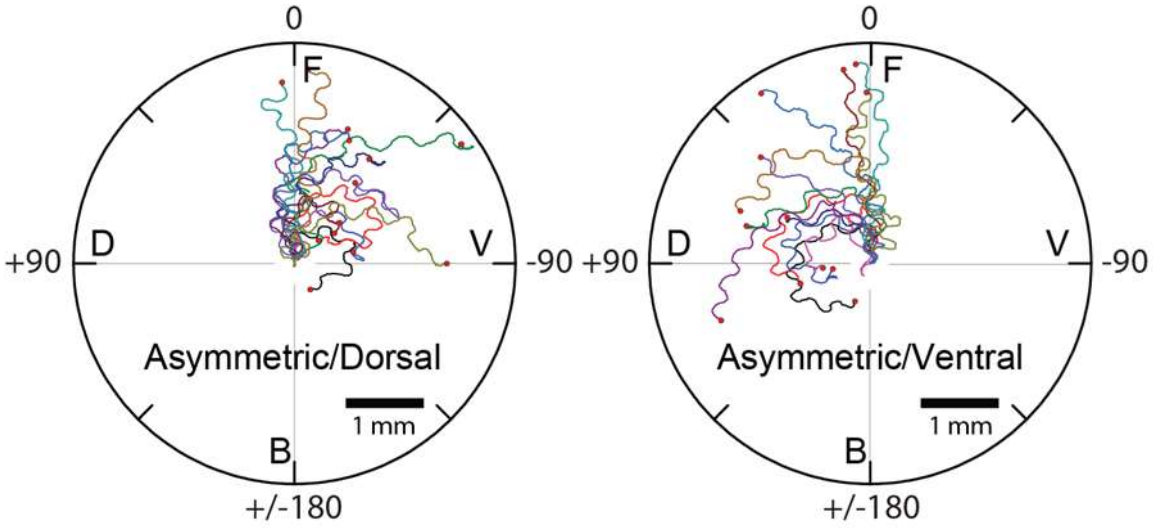

Figure 3.14: Asymmetric excitation of AIZ leads to gradual turning to the opposite side of the excitation. Sample trajectories of nose tip of animals upon dorsal (left) or ventral (right) asymmetric excitation of AIZ (n=5). The animal makes gradual turning to the opposite side of asymmetric AIZ excitation.

Using the same method, we tested if asymmetric stimulation of RIA or RIM leads to gradual turning. Asymmetric excitation of RIA does not have effects on gradual turning (Figure 3.15a-b); whereas asymmetric inhibition of RIA leads to positive turning (Figure 3.15c-d). Neither asymmetric excitation nor inhibition of RIM leads to gradual turning (Figure 3.15).

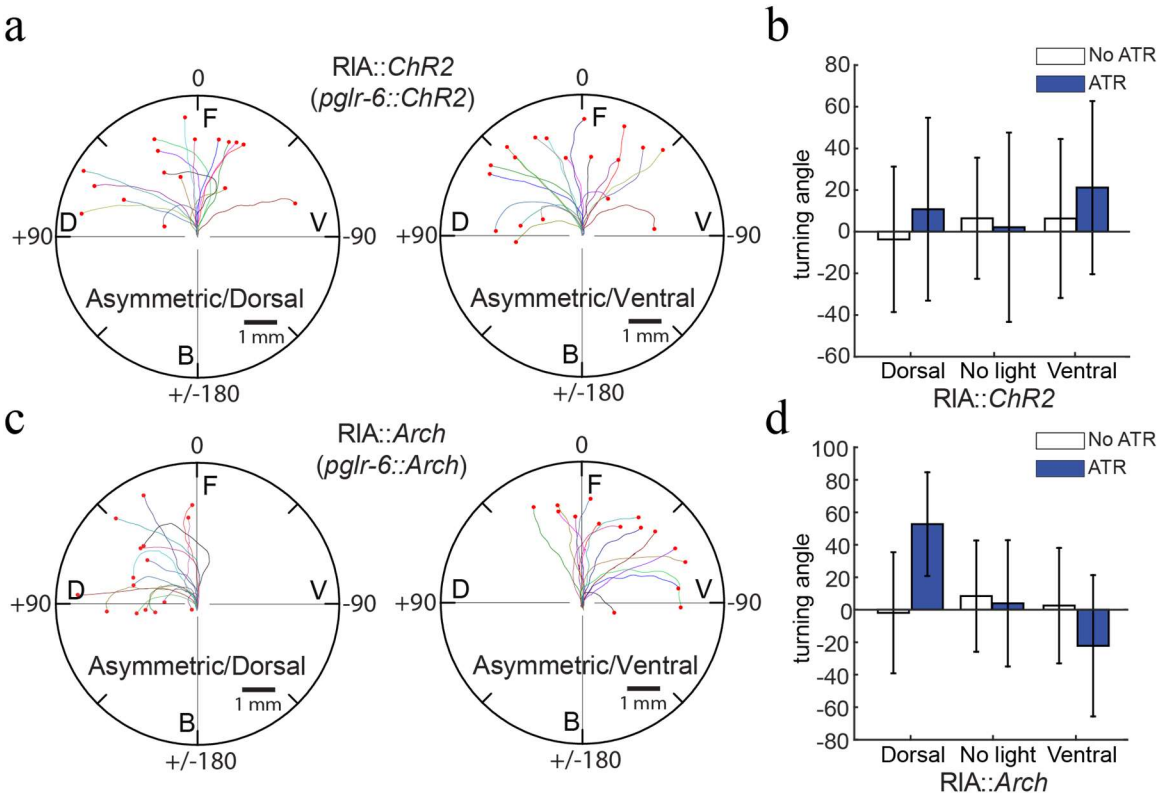

Figure 3.15: Inhibition of RIA leads to gradual turning to the same side of inhibition. **a,** Sample trajectories of center of mass of animals upon dorsal (left) or ventral (right) asymmetric excitation of RIA (n=5). **b**, Turning angle upon asymmetric excitation of RIA (n=5). Dorsal: asymmetric dorsal stimulation; no light: unstimulated; ventral: asymmetric ventral stimulation. **c**, Sample trajectories of center of mass of animals upon dorsal (left) or ventral (right) asymmetric inhibition of RIA (n=5). **d**, Turning angle upon asymmetric inhibition of RIA (n=5). Asymmetric inhibition of RIA makes the animal turn to the side of inhibition.

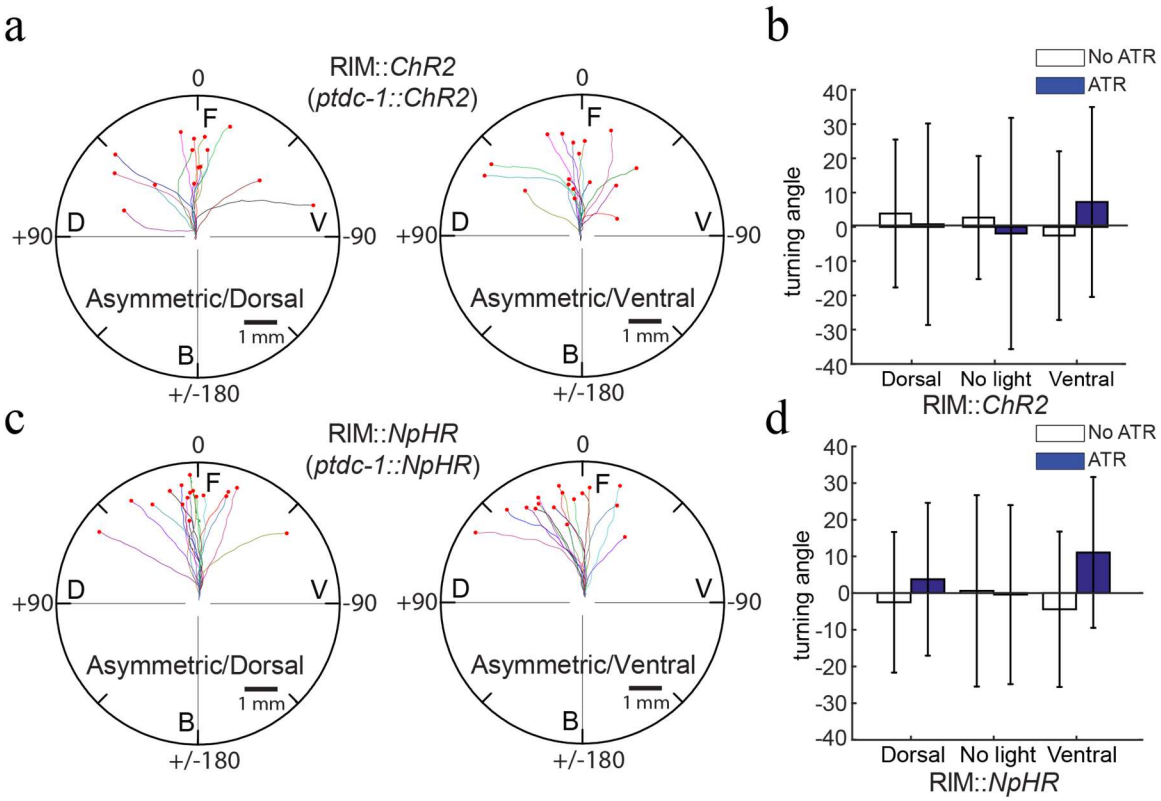

Figure 3.16: RIM asymmetric stimulation has no effect on gradual turning. a, Sample trajectories of center of mass of animals upon dorsal (left) or ventral (right) asymmetric excitation of RIM (n=5). **b**, Turning angle upon asymmetric excitation of RIM (n=5). Dorsal: asymmetric dorsal stimulation; no light: unstimulated; ventral: asymmetric ventral stimulation. **c**, Sample trajectories of center of mass of animals upon dorsal (left) or ventral (right) asymmetric inhibition of RIM (n=5). **d**, Turning angle upon asymmetric inhibition of RIM (n=5). Asymmetric excitation and asymmetric inhibition of RIM do not make the animal turn.

We used GCaMP imaging system and optogenetic stimulation to infer the role and functional connections between AIY and neurons downstream of AIY. To understand how AIY and the downstream interneurons respond to environmental stimuli, we delivered periodic bacterial odor to quantify the correlation between the activity changes of neurons and the absence or presence of odor. We also deduced the integration time of neurons by identifying the moving average time to use to obtain reversal rate to get the maxima correlation with the neural activity of neurons. Using optogenetic tools, we observed that interneurons AIZ and RIA control gradual turning and RIM control

reversals. Combining all the results, we inferred that AIY controls reversals through inhibitory connections with RIM and controls gradual turning through inhibitory connections with AIZ. The relation between AIY and RIA is more complicated and more studies are needed to understand it.

3.3. Discussion

Our results provide information about the activity patterns and functions of AIY and interneurons downstream of AIY. We can use these new findings and pre-existing literature to construct possible functional connections of neurons involved in chemotaxis (Figure 3.17). Below we will discuss how we deduced the hypothesized model and what experiments can be used to test the hypothesis.

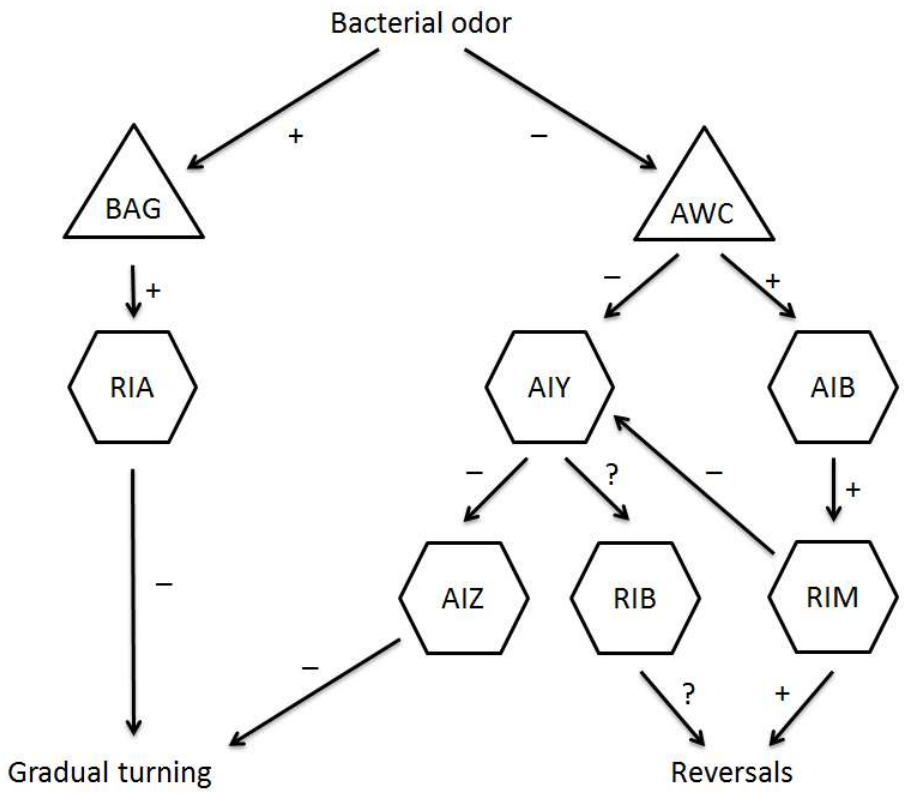

Figure 3.17: Proposed functional connections of neurons involved in chemotaxis. Triangles represent sensory neurons; hexagons represent interneurons; plus signs represent excitatory connections; minus signs represent inhibitory connections; question marks represent we do not know if the connection is excitatory or inhibitory.

3.3.1. AIY might control gradual turning through inhibition of AIZ

From the results of calcium imaging, we observed that activity of AIY is positively correlated with the presence of odor, whereas the activity of AIZ is negatively correlated with the presence of odor (Figure 3.8). Asymmetric excitation of AIY leads the animal to gradually turn towards to the side of stimulation; asymmetric excitation of AIZ leads to the opposite behavior (Figure 2.5, Figure 2.6, and Figure 3.14). Therefore, we inferred that the connections between AIY and AIZ are inhibitory since they exhibit opposite correlations with odor and opposite phenotypes upon asymmetric excitation, and therefore have opposite effects.

To test this hypothesis, we could express light-gated anti-proton pump, Archaerhodopsin-3 (Arch), to inhibit the activity of AIZ while exciting the activity of AIY asymmetrically. This is technically challenging because our current setup uses green light for tracking, which will simultaneously inhibit the activity of all neurons expressing Arch, including AIY, AIZ and other neurons. Our optical setup would need significant modification to excite one neuron and inhibit the other neuron in the nerve ring. Another approach would be to perturb the activity of AIY and observe the response of AIZ in the presence of bacterial odor. We would expect inhibition of AIY activity would lead to weak correlation of AIZ activity and bacterial odor. Since there are promoters available to express Arch only on AIY, we could use this approach to test if the odor signals are relayed to AIZ through inhibitory connections to AIY.

3.3.2. RIM might regulate the activity of AIY through secreting monoamine tyramine

AIY and RIM show opposite correlations with odor and opposite phenotypes upon symmetric excitation (Figure 3.8, Figure 3.12, and Figure 3.13). However, they only physically connect through gap junctions, which are unlikely to be inhibitory. Previous studies have shown that chemosensory neurons AWC can respond to chemoattractive odor, which in turn transmit the information to interneurons AIY and AIB. Results from Chapter 2 and previous studies showed that excitation of AIB promotes reversal behavior. Since interneurons AIB heavily connect with RIM through chemical synapses and gap junctions, it is possible that the gap junctions between AIY and RIM are inactive, but that the connections between AIB and RIM are excitatory. However, AIY and RIM could regulate the activity of each other through other means:

for example, RIM secretes monoamine tyramine and AIY expresses tyramine-gated chloride channel LGC-55. It is possible that RIM can secrete tyramine to inhibit the activity of AIY.

To test whether the gap junctions between AIY and RIM are involved in regulating activity, we could express mutants of gap junction proteins, connexons, in AIY to disrupt the gap junctions and observe the correlation of reversal rate with the activities of AIY and RIM. If the gap junctions are not involved, we would expect the result of an AIY-specific gap junction mutant to be the same as the result of wild type: activity of AIY would negatively correlate with reversal rate and activity of RIM would positively correlate with reversal rate. This result would tell us if gap junctions are important in the regulation between AIY and RIM.

To test if RIM regulates the activity of AIY through tyramine, we could either disrupt the biosynthesis of tyramine through abolishing the activity of tyrosine decarboxylase (*tdc-1*) or mutate the tyramine-gated chloride channel, LGC-55, on AIY. We would expect that the activity of RIM would still positively correlate with reversal rate, and that the negative correlation between AIY activity and reversal rate would decrease in magnitude.

3.3.3. AIY might inhibit reversals through regulating the activity of RIB

Since AIY is unlikely to control reversals through gap junctions to regulate the activity of RIM, other mechanisms might be involved. Previous studies have indicated that RIB is involved in controlling reversals and other behaviors. It is possible that AIY inhibits reversals through regulating the activity of RIB. We could not successfully use RIB-specific promoter *sto-3* to express GCaMP. It is possible that this specific condition

is toxic to *C. elegans.* We might be able to use other promoters to express GCaMP in RIB among other neurons to establish the transgenic line. Alternatively, it is possible that AIY secretes neuromodulators to regulate neurons involved in controlling reversals. Since we do not know all the neuromodulators AIY express, it will be hard to study its mechanism. We might need to develop ways to sequence RNA in single neuron AIY to identify which neuromodulators are synthesized in AIY.

Our analysis suggests that reversals can be regulated through many neurons, such as AIB, RIM and AIY discussed in here. How do they together modulate reversals based on the environmental signals they receive? It is common for neural circuits to have redundancy. This circuit might allow us to get insights in how redundant circuits compute to control a specific behavior together.

3.3.4. RIA might be regulated through BAG

The activities of both AIY and RIA are positively correlated with the presence of bacterial odor, but inhibition of AIY leads to an opposite phenotype compared to inhibition of RIA. RIA is downstream of many sensory neurons, which suggests that its activity might be regulated by multiple sources. However, odor-sensing neurons AWA, AWB and AWC either have few or no connections to RIA, which suggests that there might be other neurons that are capable of sensing odor and transmitting signals to RIA.

BAG primarily connects to RIA and RIB and is known to sense O_2 and CO_2. We measured the activity changes of BAG in response to bacterial odor and found that the activity of BAG increased upon the exposure to bacterial odor with a Pearson's correlation coefficient of 0.72 (Figure 3.18). This result suggests that the activity of RIA, which also increases during odor exposure, might be regulated by BAG instead of AIY.

We could test this hypothesis by inhibiting the activity of BAG and measuring if the correlation between RIA and bacterial odor decreases in magnitude/amplitude. There are other sensory neurons that are pre-synaptic to RIA as well, such as AUA, ADF and URX. Using similar methods, we could also test if these sensory neurons respond to bacterial odor and what they regulate. The results would extend what we know about the neurons involved in chemotaxis and give us a more complete understanding of the neural mechanisms underlying chemotaxis.

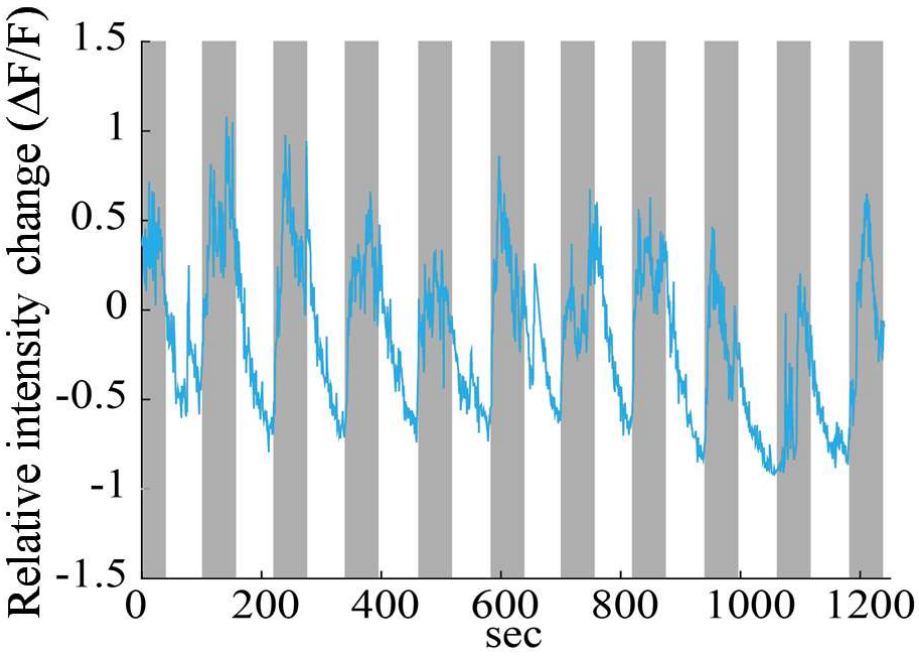

Figure 3.18: Calcium activity of BAG is positively correlated with odor. An example of the activity of BAG with the presence of odors for 60 seconds and the absence of odors for 60 seconds repeatedly. Blue line represents the activity of BAG. Grey area represents the presence of odor.

3.4. Summary

The functional connections proposed here are inferred based on literature and the experimental results we have from calcium imaging and optogenetic stimulation. The hypothesized model I presented requires replication and further validation through

experiments that more directly test association type between neurons. Among other things, we need to directly test if these neurons are indeed functionally connected. We also need to identify which receptors and what neurotransmitters and neuromodulators are involved.

Establishing a functional circuit of chemotaxis is a significant first step in understanding, but it is by no means the end of the story. After knowing how these neurons connect functionally, we can study how the circuit computes environmental stimuli to determine if the animal should move forward, reverse, or perform gradually turning. If we understand the logic of the circuit, we should be able to control important neurons to affect how the nervous system interprets the environmental stimuli to change how well the animal can perform chemotaxis. This would be a significant advance to understand chemotaxis. Furthermore, the insights we have gained from understanding chemotaxis in *C. elegans* might be powerful tools for studying more complex neural circuits in other organisms.

3.5. Method

3.5.1. Strains

Strains were grown and maintained under standard conditions[19] unless indicated otherwise. Transgenic lines with *pha-1* selection marker were grown under 24°C[20]. All experiments were done in *lite-1* mutants to minimize the animal's sensitivity to blue light[21]. A complete strain list and information on transgenes are included in the Table 3.1.

Table 3.1: Transgenic strains, genotypes, expression patterns.

Name	Genotype	Expression
SRS86	*sraIs49[nmr-1p::GCaMP3; unc-119(+)]* V *sraEx83[tdc-1p::chop-2(H134R)::mCherry; F55B11.3p::mCherry]; lite-1(ce314)* X	GCaMP: AVA, AVD, AVE mCherry: RIM, spermatheca
SRS108	*sraEx108[tdc-1p::NpHR::mKO]; lite-1(ce314)* X	mKO: RIM
SRS167	*pha-1(e2123)* III; *lite-1(ce314)* X	N/A
SRS227	*sraEx227[glr-6p::chop-2(H134R)::eYFP; F55B11.3p::mCherry]; lite-1(ce314)* X	eYFP: RIA mCherry: spermatheca
SRS228	*sraEx228[glr-6p::Arch::eGFP; F55B11.3p::mCherry]; lite-1(ce314)* X	eGFP: RIA mCherry: spermatheca
SRS467	*sraIs467[str-2p::mKO] III; lite-1(ce314)* X	AWC^{ON}
SRS656	*sraEx656 [ttx-3p::EGFP];* *sraIs467[str-2p::mKO]* III*;* *pha-1(e2123)*III*; lite-1(ce314)* X	mKO: AWC^{ON} EGFP: AIY
SRS490	*sraEx490[ttx-3p::GCaMP6s(mammalian)];* *sraIS467[str-2p::mKO]* III; *lite-1(ce314)* X	mKO: AWC^{ON} GCaMP: AIY
SRS705	*sraEx[glr-6p::GCaMP6s(C. elegans);* *ttx-3p::GCaMP6s(C. elegans)];* *sraIS467[str-2p::mKO]* III; *lite-1(ce314)* X	mKO: AWC^{ON} GCaMP: RIA, AIY
SRS676	*sraIs655[gcy-31p::GCaMP6s(C. elegans); pBX];* *sraIS467[str-2p::mKO]* III; *pha-1(e2123)* III; *lite-1(ce314)* X	mKO: AWC^{ON} GCaMP: BAG
SRS543	*sraEx543[ser-2prom2::GCaMP6s(C. elegans); pBX];* *sraIS467[str-2p::mKO]* III; *pha-1(e2123)* III; *lite-1(ce314)* X	mKO: AWC^{ON} GCaMP: AIY, AIZ, RME and other neurons
SRS621	*sraEx606[tdc-1p::GCaMP6s(C. elegans)];* *sraIS467[str-2p::mKO]* III; *pha-1(e2123)* III; *lite-1(ce314)* X	mKO: AWC^{ON} GCaMP: RIM, AIY

3.5.2. Molecular Biology

GCaMP6s optimized for mammals and *C. elegans* were cloned into Fire lab vector kit plasmid pPD96.52 (ligation number L2534, Addgene plasmid 1608). *C. elegans* codon optimized GCaMP6s was designed and *de novo* synthesized by Life Technologies. We

amplified 2kb *str-2p*, 1kb *ttx-3p,* 3.8kb *gcy-31p*, 4.4kb *tdc-1p*, 4.5kb *ser-2prom2*, 0.8kb *glr-6p* by PCR from *C. elegans* genomic DNA. All the promoters were then fused with *GCaMP, eGFP, chop-2, Arch, NpHR* or *mKO* by PCR.

3.5.3. Calcium-imaging system

L4 animals were transferred to a new NGM plate with a thin layer of *E. coli* OP50 at least an hour before experiments. Right before experiments, the animal was transferred to an open-lid, 10-cm NGM tracking plates in a water droplet to prevent damaging the worm and the agar surface. Tracking plates were moved on a leveled surface during solidification to make sure the surface even (LabExpress, Catalog No. 5001-100L). The system was operated by customized LabView scripts.

Tracking

We expressed mKO in a single neuron, AWC^{ON}, for x, y, z, and rotation tracking. Lower power 540 nm laser was used to visualize AWC^{ON} (1.75 mW/mm^2) at magnification of 44X. As the animal swings its head, the position of AWC^{ON} changes and rotates quickly. We used fast computation using field-programmable gate arrays (FPGA, National Instruments) to compute the position of the neuron and compensated the displacement with x, y, z and rotation mechanical stages. Position changes in x and y were calculated based on the displacement between the center of mass of AWC^{ON} and the center of the field of view. Z displacement was calculated based on the intensity of AWC^{ON} in two different focal planes created by a defocus lens (Figure 3.1). The displacements of x, y and z were compensated by servo and piezo stages (Newport and Physik Instrumente, respectively). Rotation offset was calculated from the principal angle of the process of AWC^{ON}, which then was compensated by a dove prism. These feedback loops from

measurement, computation to mechanical movement were operated at 100 times per second to achieve a 5-μm resolution of tracking AWC^{ON} in a freely moving animal.

GCaMP imaging

The resolution of the tracking feedback loop allows us to use long exposure times to measure GCaMP intensity. We used 80 μW blue LED at the magnification of 50X by an EMCCD camera at 15.625 frames per second. It is crucial to use light power less than 160 μW for imaging which otherwise disrupts the animal's behavior. We used a tunable lens to change the focal plane so that we can image calcium activity from neurons in different depths.

Body posture recording

Dark-field 660 nm illumination was used to visualize the posture of the animal under 1X magnification by a Thorlabs camera at 9.8 Hz.

Odor delivery

An electric three way valve (The Lee Company) was used to determine whether the air (30 SCCM) was bubbled through water or saturated bacteria liquid culture.

Analysis

Data were then analyzed by customized Matlab scripts. GCaMP intensity was measured by searching for the brightest pixel within neurons of interest. It was then normalized by the median of the smoothed GCaMP intensity. Trajectories of the animal were obtained by the information from both the servo and piezo stages. They were then smoothed with 30 μm resolution. Reversals were identified based on the angle of the smoothed trajectory.

3.5.4. Correlation analysis of odor pulsing

Data were analyzed by customized Matlab scripts. The slow modulation of the GCaMP intensity was first subtracted so that only the modulation in the frequency of interest was studied. The data were then rescaled and correlated with odor signals by Pearson's correlation. Lag time was calculated by calculating the Pearson's correlation between the circular shifted data and odor signals. The result was then compared with the distribution calculated from the Pearson's correlation between 400 randomly permuted matrices from the data and odor signals. The result was considered statistically significant if the correlation coefficient is more than two standard deviations away from the histogram.

3.5.5. Chemotaxis assay

Bacterial lawn was prepared with saturated liquid *E. coli* OP50 culture grown overnight. The bacterial lawn was seeded in an open-lid, 10-cm NGM tracking plates within 10 minutes before an experiment started. L4 animals were transferred to a new NGM plate with a thin layer of *E. coli* OP50 at least an hour before experiments. The animal was transferred to chemotaxis plate in a water droplet to prevent damaging the worm and the agar surface.

References

1. Kocabas, A., Shen, C.-H., Guo, Z. V & Ramanathan, S. Controlling interneuron activity in Caenorhabditis elegans to evoke chemotactic behaviour. *Nature* **490,** 273–7 (2012).

2. White, J. G., Southgate, E., Thomson, J. N. & Brenner, S. The Structure of the Nervous System of the Nematode Caenorhabditis elegans. *Phil. Trans. Royahl Soc. Lond. B* **314,** 1–340 (1986).

3. Faumont, S. *et al.* An image-free opto-mechanical system for creating virtual environments and imaging neuronal activity in freely moving Caenorhabditis elegans. *PloS one* **6,** e24666 (2011).

4. Luo, L. *et al.* Dynamic encoding of perception, memory, and movement in a C. elegans chemotaxis circuit. *Neuron* **82,** 1115–28 (2014).

5. Larsch, J., Ventimiglia, D., Bargmann, C. I. & Albrecht, D. R. High-throughput imaging of neuronal activity in Caenorhabditis elegans. (2013). doi:10.1073/pnas.1318325110/-/DCSupplemental.www.pnas.org/cgi/doi/10.1073/pnas.1318325110

6. Chen, T.-W. *et al.* Ultrasensitive fluorescent proteins for imaging neuronal activity. *Nature* **499,** 295–300 (2013).

7. Tian, L. *et al.* Imaging neural activity in worms, flies and mice with improved GCaMP calcium indicators. *Nature methods* **6,** 875–81 (2009).

8. Chalasani, S. H. *et al.* Dissecting a circuit for olfactory behaviour in Caenorhabditis elegans. *Nature* **450,** 63–70 (2007).

9. Chang, S., Johnston, R. J. & Hobert, O. A transcriptional regulatory cascade that controls left/right asymmetry in chemosensory neurons of C. elegans. *Genes & development* **17,** 2123–37 (2003).

10. Peckol, E. L., Troemel, E. R. & Bargmann, C. I. Sensory experience and sensory activity regulate chemosensory receptor gene expression in Caenorhabditis elegans. *Proceedings of the National Academy of Sciences of the United States of America* **98,** 11032–8 (2001).

11. Karasawa, S., Araki, T., Nagai, T., Mizuno, H. & Miyawaki, A. Cyan-emitting and orange-emitting fluorescent proteins as a donor / acceptor. *Society* **312,** 307–312 (2004).

12. Schultheis, C., Brauner, M., Liewald, J. F. & Gottschalk, A. Optogenetic analysis of GABAB receptor signaling in Caenorhabditis elegans motor neurons. *Journal of neurophysiology* **106,** 817–27 (2011).

13. Kawano, T. *et al.* An imbalancing act: gap junctions reduce the backward motor circuit activity to bias C. elegans for forward locomotion. *Neuron* **72,** 572–86 (2011).

14. Guo, Z. V, Hart, A. C. & Ramanathan, S. Optical interrogation of neural circuits in Caenorhabditis elegans. *Nature methods* **6,** 891–6 (2009).

15. Tsalik, E. LIM homeobox gene-dependent expression of biogenic amine receptors in restricted regions of the C. elegans nervous system. *Developmental Biology* **263,** 81–102 (2003).

16. Brockie, P. J., Mellem, J. E., Hills, T., Madsen, D. M. & Maricq, a V. The C. elegans glutamate receptor subunit NMR-1 is required for slow NMDA-activated currents that regulate reversal frequency during locomotion. *Neuron* **31,** 617–30 (2001).

17. Jin, L. *et al.* Single action potentials and subthreshold electrical events imaged in neurons with a fluorescent protein voltage probe. *Neuron* **75,** 779–85 (2012).

18. Cao, G. *et al.* Genetically targeted optical electrophysiology in intact neural circuits. *Cell* **154,** 904–13 (2013).

19. Brenner, S. & Ls, D. P. F. J. The genetics of behaviour. *Prospects* **29,** 269–271

20. Granato, M., Schnabel, H., Schnabel, R., Biochemie, M. & A, A. K. selectable marker for transfer in C . elegans. *Science* **22,** 1762–1763 (1994).

21. Edwards, S. L. *et al.* A novel molecular solution for ultraviolet light detection in Caenorhabditis elegans. *PLoS biology* **6,** e198 (2008).

Chapter 4. Discussion

In this thesis, we identified important neurons and activity patterns involved in chemotaxis in *C. elegans* by perturbing and measuring the activity of them in freely moving animals. However, the neurons and patterns we identified are only part of the story. To more completely understand the neural basis of any complex behavior, including chemotaxis, there are three questions we must ask.

4.1. What are the neurons involved in chemotaxis?

To understand chemotaxis or any complex behavior comprehensively, we need to identify all neurons that control the behaviors involved in chemotaxis. Previous studies have found, through ablation, around 20 classes of neurons that appear important in navigation and chemotaxis[1–5]. The standard approach is to kill neurons of interest from L1-stage larvae with laser beams and test the behavioral defects of the animals when they become young adults[6]. It has been extremely useful for examining the roles of neurons in behaviors of interest. However, ablating the same neurons in different larval stages have different behavioral phenotypes, suggesting that the nervous system might compensate the functions of the ablated neurons during development[7]. There are also no ways to verify if neurons near the ablated target are damaged. These issues thus complicate the interpretation of the results. Even if we can correctly ablate neurons of interest and demonstrate there are no side effects, this approach is labor-intensive and difficult to scale up for large sample sizes.

To study the effects of particular neurons, we would ideally ablate neurons of interest in many worms and quantify changes in behavior in the same worms before and after ablation. Fluorescent proteins, such as KillerRed and miniSOG, have been

developed to ablate neurons with temporal and spatial precision[8–11]. However, light is potentially damaging to *C. elegans*[12] and these florescent proteins can induce strong phototoxicity and require 30 minutes to an hour of exposure to ablate the neurons. It can therefore be difficult to determine whether behavioral differences before and after photoablation derive from intentionally ablated neurons or from light damaging of the animal. Florescent proteins such as KillerRed and miniSOG would be more useful to this type of research if the necessary time or amount of light exposure is decreased to seconds to minimize light damages to the worm.

Another possibility to determine important neurons for chemotaxis is to use optogenetics to temporarily perturb neurons of interest and study the associated behavioral phenotypes. We can express light-gated ion channels such as channelrhodopsin-2 (ChR2) and archaerhodopsin-3 (Arch) in neurons of interest[13–16], illuminate these neurons on multiple animals simultaneously, thereby hyperpolarizing or depolarizing the function of the neurons, and then compare the behaviors of those animals before, during and after perturbation. The perturbation in this approach is temporary and reversible and is less likely to affect the development of nervous system. This approach can also allow us to characterize the neurons' roles in chemotaxis more quickly because we can scale up to study many animals at a time.

Previous postdoctoral fellow Dr. Josselin Milloz and I with analysis assistance from graduate student Jeffrey Lee used this method to inhibit small sets of neurons at controlled duration while the animals chemotaxed toward food. Together we targeted most sensory neurons and interneurons in *C. elegans* at least once. We found that some transgenic animals chemotax poorly during perturbation. These animals exhibit different

locomotion behavior during perturbation compared to animals without inhibition, quantified by differences in reversal frequencies, velocities or turning behaviors. The simplest hypothesis is to assume these animals cannot chemotax due to locomotion defects. However, we also found counter examples where some animals with similar locomotion defects during perturbation still successfully chemotaxed to the bacterial lawn, given enough time. This suggests that animals with locomotion defects can still reach the bacterial lawn as long as the animal can correctly sense and compute where to find the food. For the animals that are completely defective in chemotaxis, there are two possible scenarios: (1) the motor programs are all defective and therefore the animals cannot reach the food even if the neurons for sensing and computing are not affected; or (2) the animals might have problems in sensing or computing and therefore cannot control the motor programs to move towards the lawn. To figure out why the animals cannot find food, we will need to measure the activity of these neurons during chemotaxis and analyze if their activities are correlated with behaviors or processing sensory information. The transgenic lines we created can be used to screen for important neurons in all sorts of behavior in *C. elegans.* Similar approach can also be adapted to other organisms to identify neurons involved in different behaviors.

This approach assumes that there is little redundancy in the neural circuit. However, it is likely that one needs to inhibit many neurons in the circuit to observe abnormal phenotypes. There are millions of combinations to inhibit sets of neurons. If we do not have prior knowledge which neurons are important, we will never be able to find the right neurons to study. Even if we found the right combination, we will have a hard time to identify the neurons once Arch is expressed on more than 5 pairs of neurons. In

addition, the transgenic construct is in extrachromosomal array and might not be stable. There can be mosaic expression of Arch, which makes the interpretation even harder.

We also need to ask if it is necessary to identify all neurons involved in chemotaxis to understand chemotaxis. It is possible that some neurons control and coordinate all neurons downstream of them. Once we understand how these neurons compute, we can predict how well the animal perform chemotaxis. In this case, we should spend more time thinking how to identify these neurons than performing a screen to identify all neurons involved in chemotaxis.

4.2. How to characterize behaviors that are independent and physiologically relevant?

Another way to study chemotaxis is to examine it from a behavioral perspective. First, we need to develop objective ways to characterize behaviors involved in chemotaxis. A behavior is an animal's response to external environmental stimuli based on the animal's internal state. However, even seemingly simple behaviors are in reality complex and ambiguously classified; "reversals," for example, can vary in the duration of backward movement, the angle of reorientation, and whether or not the reversal occurs after an omega turn. Defining reversals or other behaviors based on the empirical description is problematic. The definition cannot be comprehensively quantified and is subjected to experimenters' interpretation. Alternatively, previous studies represented the animal's posture with four fundamental shapes and derived "behavioral motifs" by unsupervised computer learning algorithms[17,18]. This method revealed phenotypes that were not detected by manual observation. But it is unclear if any of the behavioral motifs reflect how the nervous system controls behaviors.

Ideally, we would like to characterize behaviors so that they are independent of each other and are physiologically relevant. Since all behaviors in an animal are controlled by its nervous system, we can cluster neurons that show strong correlated neural activity and ask how the activity changes correlate with the animal's movement to derive the simplest neural description of behaviors. To achieve that, we can measure all the neurons at once while the animal is freely moving and develop methods to identify individual neurons. The neurons in *C. elegans* are hard to resolve as they are densely packed in the nerve ring. Researchers have used nucleus-localized genetically encoded calcium indicators for whole-brain imaging[19]. However, it is unclear how the calcium activity changes in the nucleus are associated to changes in neural activity. Alternatively, since an animal's locomotion is controlled by motor neurons, we can start by characterizing which motor neurons work together and what behaviors they control. After characterizing behaviors based on neural activities, we can study how neurons upstream of motor neurons compute external cues and relay the signals to motor neurons to control the animal's behaviors. Starting from simple behaviors and working our way upstream is a powerful way to study the neuroscience of complex behaviors.

This approach assumes that the motor neurons are controlled by neurons that are physically connected through chemical synapses or gap junctions. However, the activity of motor neurons can also be regulated through neuromodulators, which can be secreted by any neurons in the nervous system. One way to overcome it is to know which receptors are expressed on motor neurons. However, there are technical challenges to dissociate single neurons for RNA sequencing on single neuron in *C. elegans*. Even if we overcome the challenges, it is a big undertaking to sequence all the motor neurons,

understand their receptor expression profile and determine what other neurons we should study.

4.3. How does the nervous system regulate long-lasting behaviors?

An animal can organize a sequence of behaviors to form a long-lasting behavior. During chemotaxis, a *C. elegans* modulates its behaviors to switch between local and long range search[3–5,20]. Animals in local search reverse frequently and move within a small area; whereas animals in long range search have low reversal frequency and therefore can explore larger areas. An animal can switch between both searching strategies based on its distance to food source and how long it has been removed from food. This behavior modulation suggests that the nervous system can integrate information from environmental cues and internal states to switch between different behavioral states. How does the nervous system sustain long-lasting behaviors and switch between them?

Previous studies have shown that neurotransmitters and neuromodulators are important in regulating long-lasting behaviors[20–24]. For example, serotonergic signaling and neuropeptide pigment dispersing factors (PDF) are involved in regulating reversal frequency between low and high frequencies in the presence of food[23]. Dopaminergic and glutamatergic signalings are important in controlling local search[20]. However, it is unclear how the nervous system uses the neurotransmitters and neuromodulators to regulate the long-lasting behaviors.

The nervous system needs to sustain long-lasting behaviors and switch between them. Therefore, we can identify candidate neurons by screening for animals with abnormal duration of the long-lasting behaviors during perturbation. We can study the

functions of the neurons through calcium imaging. For example, the activity of neurons involved in sustaining the behavior should be correlated with the behavior. On the other hand, if we monitor the activity of neurons responsible for switching between different long-lasting behaviors, we would expect activity changes of the neuron when the animal switches the behavior.

Among the neurons we have examined in the thesis, interneurons AIY might be involved in regulating long-lasting behaviors. Animals exhibit lower reversal frequency (long-range search) during AIY excitation and higher reversal frequency (local search) during AIY inhibition[1,5,25]. We also observed that activity levels of interneurons AIY can sustain for several minutes and correlate with reversal rate of the animal. These results suggest that AIY might be involved to regulate the long-lasting behaviors of the animal. Next we will need to identify the neurotransmitters or neuromodulators that regulate the activity levels of AIY. Interneurons AIY have receptors for glutamate (MGL-1, GLC-3), dopamine (DOP-1, DOP-3), serotonin (MOD-1), and PDF (PDFR)[23,26–29]. In animals with defects in secreting glutamate, dopamine, serotonin or PDF, we can study whether the activity of AIY is perturbed and if the activity changes lead to behavioral changes. Based on which neurotransmitters or neuromodulators are involved, we can further study which neurons control the activity of AIY. These neurons can provide information of how the nervous system switches and sustains between different long-lasting behaviors.

However, there can be dozens of neurons that show long-lasting activity changes as AIY and many neurotransmitters and neuromodulators are involved. In this case, our knowledge of how these neurons physically connect would not be useful.

The dynamics of the receptors can also be complicated. How would you discern the effect of one receptor from the other?

4.4. Limitations of current techniques

4.4.1. We cannot perturb or image activity locally in specific synapses

Electrophysiology studies have shown that neurons in *C. elegans* are iso-potential, suggesting that most activities occur locally in processes[30]. As a result, it is possible that we miss crucial information about neurons by perturbing or imaging activity in the soma or process non-specifically. However, since we can evoke consistent behavioral changes by perturbing the activity of a whole neuron and can consistently correlate behaviors with neural activity of either the soma or the process, it seems that our method still gives us meaningful information about the function or behavior that the neuron regulates.

4.4.2. Calcium activity might not be a good proxy for fast neural dynamics.

In our studies, we did not observe fast calcium activity changes through our optical system. There are several possibilities for why this is the case: (1) the dynamics of neuronal activity in the neurons we measured are indeed slow; (2) the dynamics of calcium influx or of GCaMP is slow; (3) the amplitude of GCaMP changes in fast dynamics is out of our detection limit. The most direct way to examine if fast neural dynamics exist is by directly measuring voltage change rather than changes in calcium activity. However, the available methods for measuring voltage change do not look promising for this application using our setup.

Arch(D95N) is one of the best genetically encoded fluorescence voltage indicators available[31]. I tested the dynamic range of Arch(D95N) in various neurons in *C. elegans* in collaboration with Dr. Adam Cohen's lab. The highest result we saw was a 5%

change of ΔF/F in motor neurons under red laser illumination (3 W/mm^2). Since our current optical system can only resolve changes over 20% ΔF/F, we cannot resolve the voltage changes with current fluorescence voltage indicators. The current power level of red laser is also too high and therefore might damage the worm. The results from imaging fluorescence changes of voltage-sensitive dye are not promising either, because the maxima changes of fluorescence are within few percent, which is still below our detection limit and currently there are no viable ways to deliver fluorescent dyes to the nervous system of *C. elegans*. Therefore, we do not currently have good alternatives to the genetically-encoded calcium indicators, such as GCaMP that we currently use. It is desirable to improve the signal amplitude and the signal to noise ratio of current genetically encoded voltage sensors. Once we can monitor voltage changes in freely behaving *C. elegans,* it will be a powerful tool to understand how neurons sense environment, compute signals and control behaviors.

4.5. Summary

Even though *C. elegans* only has 302 neurons, many basic concepts are still not understood: How can we identify all neurons involved in regulating a given behavior? How should we define a behavior? What is the neural mechanism to sustain and switch between long-lasting behaviors?

Researchers working on other organisms have also started to tackle similar challenges. For example, Voeglstein, Park and Ohyama *et al*. developed an optogenetic activation screen to record behaviors of 1054 *Drosophila* larval lines[32]. They used computer algorithms to classify the behavioral response (behaviotype) during the activation and built a “neuron line-behaviotype atlas”. One can use these lines to screen

for neurons involved in long-lasting behaviors, such as sleep-wake cycle and memory. One limitation of the approach is that we do know how neurons connect in *Drosophila* larvae. Understanding how these neurons connect will be informative to test how a specific neural circuit works.

Another example is from studies in larval zebrafish. Ahrens *et al*. demonstrated the ability to use light-sheet microscopy to record activity of around 80% of neurons from an entire larval brain at 0.8 Hz[33]. Even though the animal has to be stationary, this technique can be combined with a "fictive virtual-reality setup" to correlate activity of neurons and fictive behaviors[34]. Using this approach, one can identify important neurons for behaviors of interest and cluster activity of neurons to define behaviors so that they are orthogonal to each other. The challenge of the system is to justify that the brain activity in a fictive swim is physiologically similar to the condition when the animal swims freely.

Compared with other organisms, *C. elegans* has the advantage of having a wiring diagram describing the physical connections between neurons and tools to perturb and image neural activity in freely moving animals. It also exhibits complex behaviors, such as chemotaxis, that involve sensing, computing and behaving at a variety of time scales. We already have tools available help us understand what we might need to fully map a circuit, to define a behavior, and to study long-lasting behaviors. The insights we learn from *C. elegans* can be used to guide what approaches are feasible and what tools we should develop in other organisms to address these basic questions.

References

1. Tsalik, E. L. & Hobert, O. Functional mapping of neurons that control locomotory behavior in Caenorhabditis elegans. *Journal of neurobiology* **56,** 178–97 (2003).

2. Iino, Y. & Yoshida, K. Parallel use of two behavioral mechanisms for chemotaxis in Caenorhabditis elegans. *The Journal of neuroscience : the official journal of the Society for Neuroscience* **29,** 5370–80 (2009).

3. Pierce-Shimomura, J. T., Morse, T. M. & Lockery, S. R. The fundamental role of pirouettes in Caenorhabditis elegans chemotaxis. *The Journal of neuroscience : the official journal of the Society for Neuroscience* **19,** 9557–69 (1999).

4. Wakabayashi, T., Kitagawa, I. & Shingai, R. Neurons regulating the duration of forward locomotion in Caenorhabditis elegans. *Neuroscience research* **50,** 103–11 (2004).

5. Gray, J. M., Hill, J. J. & Bargmann, C. I. A circuit for navigation in Caenorhabditis elegans. *Proceedings of the National Academy of Sciences of the United States of America* **102,** 3184–91 (2005).

6. Bargmann, C. I. & Avery, L. Laser killing of cells in Caenorhabditis elegans. *Methods in cell biology* **48,** 225–50 (1995).

7. White, J. Q. *et al.* The sensory circuitry for sexual attraction in C. elegans males. *Current biology : CB* **17,** 1847–57 (2007).

8. Teh, C. *et al.* Optogenetic in vivo cell manipulation in KillerRed-expressing zebrafish transgenics. *BMC developmental biology* **10,** 110 (2010).

9. Kobayashi, J. *et al.* A method for selective ablation of neurons in C. elegans using the phototoxic fluorescent protein, KillerRed. *Neuroscience Letters* **548,** 261–264 (2013).

10. Qi, Y. B., Garren, E. J., Shu, X., Tsien, R. Y. & Jin, Y. Photo-inducible cell ablation in Caenorhabditis elegans using the genetically encoded singlet oxygen generating protein miniSOG. *Proceedings of the National Academy of Sciences of the United States of America* **109,** 7499–504 (2012).

11. Lin, J. Y. *et al.* Optogenetic Inhibition of Synaptic Release with Chromophore-Assisted Light Inactivation (CALI). *Neuron* **79,** 241–53 (2013).

12. Edwards, S. L. *et al.* A novel molecular solution for ultraviolet light detection in Caenorhabditis elegans. *PLoS biology* **6,** e198 (2008).

13. Nagel, G. *et al.* Channelrhodopsin-2, a directly light-gated cation-selective membrane channel. *Proceedings of the National Academy of Sciences of the United States of America* **100,** 13940–5 (2003).

14. Nagel, G. *et al.* Light activation of channelrhodopsin-2 in excitable cells of Caenorhabditis elegans triggers rapid behavioral responses. *Current biology : CB* **15,** 2279–84 (2005).

15. Boyden, E. S., Zhang, F., Bamberg, E., Nagel, G. & Deisseroth, K. Millisecond-timescale, genetically targeted optical control of neural activity. *Nature neuroscience* **8,** 1263–8 (2005).

16. Okazaki, A., Sudo, Y. & Takagi, S. Optical silencing of C. elegans cells with arch proton pump. *PloS one* **7,** e35370 (2012).

17. Brown, A. E. X., Yemini, E. I., Grundy, L. J., Jucikas, T. & Schafer, W. R. A dictionary of behavioral motifs reveals clusters of genes affecting Caenorhabditis elegans locomotion. *Proceedings of the National Academy of Sciences of the United States of America* **110,** 791–6 (2013).

18. Stephens, G. J., Johnson-Kerner, B., Bialek, W. & Ryu, W. S. Dimensionality and Dynamics in the Behavior of C. elegans. *PLoS Computational Biology* **4,** e1000028 (2008).

19. Schrödel, T., Prevedel, R., Aumayr, K., Zimmer, M. & Vaziri, A. Brain-wide 3D imaging of neuronal activity in Caenorhabditis elegans with sculpted light. *Nature methods* (2013). doi:10.1038/nmeth.2637

20. Hills, T., Brockie, P. J. & Maricq, A. V. Dopamine and glutamate control area-restricted search behavior in Caenorhabditis elegans. *The Journal of neuroscience : the official journal of the Society for Neuroscience* **24,** 1217–25 (2004).

21. Kim, K. & Li, C. Expression and regulation of an FMRFamide-related neuropeptide gene family in Caenorhabditis elegans. *The Journal of comparative neurology* **475,** 540–50 (2004).

22. Sawin, E. R., Ranganathan, R. & Horvitz, H. R. C . elegans Locomotory Rate Is Modulated by the Environment through a Dopaminergic Pathway and by Experience through a Serotonergic Pathway. **26,** 619–631 (2000).

23. Flavell, S. W. *et al.* Serotonin and the Neuropeptide PDF Initiate and Extend Opposing Behavioral States in C. elegans. *Cell* **154,** 1023–35 (2013).

24. Pirri, J. K., McPherson, A. D., Donnelly, J. L., Francis, M. M. & Alkema, M. J. A tyramine-gated chloride channel coordinates distinct motor programs of a Caenorhabditis elegans escape response. *Neuron* **62,** 526–38 (2009).

25. Kocabas, A., Shen, C.-H., Guo, Z. V & Ramanathan, S. Controlling interneuron activity in Caenorhabditis elegans to evoke chemotactic behaviour. *Nature* **490,** 273–7 (2012).

26. Tsalik, E. LIM homeobox gene-dependent expression of biogenic amine receptors in restricted regions of the C. elegans nervous system. *Developmental Biology* **263,** 81–102 (2003).

27. Greer, E. R., Pérez, C. L., Van Gilst, M. R., Lee, B. H. & Ashrafi, K. Neural and molecular dissection of a C. elegans sensory circuit that regulates fat and feeding. *Cell metabolism* **8,** 118–31 (2008).

28. Wenick, A. S., Hobert, O. & York, N. Genomic cis-Regulatory Architecture and trans-Acting Regulators of a Single Interneuron-Specific Gene Battery in C . elegans. **6,** 757–770 (2004).

29. Harris, G. P. *et al.* Three Distinct Amine Receptors Operating at Different Levels within the Locomotory Circuit Are Each Essential for the Serotonergic Modulation of Chemosensation in Caenorhabditis elegans. *Journal of Neuroscience* **29,** 1446–1456 (2009).

30. Goodman, M. B., Hall, D. H., Avery, L. & Lockery, S. R. and Dynamic Range in C . elegans Neurons. **20,** 763–772 (1998).

31. Kralj, J. M., Douglass, A. D., Hochbaum, D. R., Maclaurin, D. & Cohen, A. E. Optical recording of action potentials in mammalian neurons using a microbial rhodopsin. *Nature methods* **9,** 90–5 (2012).

32. Vogelstein, T., Truman, J. W., Priebe, C. E. & Zlatic, M. Discovery of Brainwide Neural- Behavioral Maps via Multiscale Unsupervised Structure Learning. 1–9

33. Ahrens, M. B., Orger, M. B., Robson, D. N., Li, J. M. & Keller, P. J. Whole-brain functional imaging at cellular resolution using light-sheet microscopy. **10,** (2013).

34. Ahrens, M. B. *et al.* Brain-wide neuronal dynamics during motor adaptation in zebrafish. *Nature* **485,** 471–7 (2012).